

**UNIVERSITÄTSKLINIKUM HAMBURG-EPPENDORF**

Klinik und Poliklinik für Diagnostische und Interventionelle Radiologie

Prof. Dr. med. Gerhard Adam

**Molecular imaging of tumors with nanobodies and antibodies:  
Timing and dosage are crucial factors for improved *in vivo* detection**

**Dissertation**

zur Erlangung des Grades eines Doktors der Medizin  
an der Medizinischen Fakultät der Universität Hamburg.

vorgelegt von:

Alexander Lenz

aus Lutherstadt Wittenberg

Hamburg 2016

**Angenommen von der  
Medizinischen Fakultät der Universität Hamburg am: 23.08.2016**

**Veröffentlicht mit Genehmigung der  
Medizinischen Fakultät der Universität Hamburg**

**Prüfungsausschuss, der/die Vorsitzende:** Prof. Dr. G. Adam

**Prüfungsausschuss, zweite/r Gutachter/in:** Prof. Dr. F. Nolte

**Prüfungsausschuss, dritte/r Gutachter/in:**

## **Table of contents**

### **1. Paper**

1.1. Supplementary tables and figures

### **2. Summary and description of paper**

2.1 References

### **3. Abstract**

### **4. Explanation of own contribution**

### **5. Acknowledgements**

### **6. Curriculum Vitae**

### **7. Publications**

### **8. Eidesstattliche Erklärung (Affidavit)**

# Molecular imaging of tumors with nanobodies and antibodies: Timing and dosage are crucial factors for improved *in vivo* detection

Peter Bannas<sup>a,\*†</sup>, Alexander Lenz<sup>a,b†</sup>, Valentin Kunick<sup>a,b</sup>, Lennart Well<sup>a,b</sup>, William Fumey<sup>a,b</sup>, Björn Rissiek<sup>b,c</sup>, Friedrich Haag<sup>b</sup>, Joanna Schmid<sup>a,b</sup>, Kerstin Schütze<sup>a,b</sup>, Anna Eichhoff<sup>b</sup>, Martin Trepel<sup>d</sup>, Gerhard Adam<sup>a</sup>, Harald Ittrich<sup>a</sup> and Friedrich Koch-Nolte<sup>b</sup>



The utility of nanobodies and conventional antibodies for *in vivo* imaging is well known, but optimum dosing and timing schedules for one versus the other have not been established. We aimed to improve specific tumor imaging *in vivo* with nanobodies and conventional antibodies using near-infrared fluorescence (NIRF) imaging. We used ARTC2 expressed on lymphoma cells as a model target antigen. ARTC2-specific nanobody s+16a and conventional antibody Nika102 were labeled with NIRF-dye AF680. *In vivo* NIRF-imaging of ARTC2-positive and ARTC2-negative xenografts was performed over 24 h post-injection of 5, 10, 25, or 50 µg of each conjugate. Specific target-binding and tissue-penetration were verified by NIRF imaging *ex vivo*, flow cytometry and fluorescence microscopy. NIRF-imaging of s+16a<sup>680</sup> *in vivo* revealed a six times faster tumor accumulation than of Nika102<sup>680</sup>. Using 50 µg of s+16a<sup>680</sup> increased the specific signals of ARTC2-positive tumors without increasing background signals, allowing a tumor-to-background (T/B) ratio of  $12.4 \pm 4.2$  within 6 h post-injection. Fifty micrograms of Nika102<sup>680</sup> increased specific signals of ARTC2-positive tumors but also of ARTC2-negative tumors and background, thereby limiting the T/B ratio to  $6.1 \pm 2.0$ . Ten micrograms of Nika102<sup>680</sup> only slightly reduced specific tumor signals but dramatically reduced background signals. *Ex vivo* analyses confirmed a faster and deeper tumor penetration with s+16a<sup>680</sup>. Using nanobody s+16a allowed same-day imaging with a high T/B ratio, whereas antibody Nika102 gave optimal imaging results only 24 h post injection. Nanobody s+16a required a high dose, whereas antibody Nika102 had the best T/B-ratio at a low dose. Therefore, timing and dosage should be addressed when comparing nanobodies and conventional antibodies for molecular imaging purposes. Copyright © 2015 John Wiley & Sons, Ltd.

Additional supporting information may be found in the online version of this article at the publisher's web site.

**Keywords:** Nanobody; antibody; VHH; fluorescence imaging; molecular imaging; xenograft; animal model

## 1. INTRODUCTION

*In vivo* molecular imaging focuses on the non-invasive detection and characterization of target structures with specific probes (1,2). Based on their unmatched binding specificity and affinity, monoclonal antibodies are considered the most specific probes for targeted imaging (3–5). However, their preclinical and clinical utility is limited due to their relatively poor and slow tissue penetration, slow clearance from circulation, and long retention in non-targeted tissues (6). These characteristics impair their signal-to-background ratio (7). The development of new contrast agents and novel engineered forms of antibodies, such as diabodies, minibodies, single-chain variable fragments, and nanobodies, has triggered a new wave of antibody-based imaging approaches (3,5,6,8). Among these, nanobodies are the smallest available antigen-binding fragments derived from camelid heavy-chain-only antibodies (9,10). With only ~15–18 kDa, these small antibody fragments are soluble, very stable and are renally cleared from the circulation (9,11). These properties make them particularly suited for specific and efficient targeting of tumor antigens *in vivo* (12–20).

\* Correspondence to: Peter Bannas, University Medical Center Hamburg-Eppendorf, Department of Radiology, Martinistrasse 52, 20246 Hamburg, Germany. E-mail: p.bannas@uke.de

† These authors contributed equally.

a P. Bannas, A. Lenz, V. Kunick, L. Well, W. Fumey, J. Schmid, K. Schütze, G. Adam, H. Ittrich  
Department of Diagnostic and Interventional Radiology, University Medical Center Hamburg-Eppendorf, Hamburg, Germany

b A. Lenz, V. Kunick, L. Well, W. Fumey, B. Rissiek, F. Haag, J. Schmid, K. Schütze, A. Eichhoff, F. Koch-Nolte  
Institute of Immunology, University Medical Center Hamburg-Eppendorf, Hamburg, Germany

c B. Rissiek  
Department of Neurology, University Medical Center Hamburg-Eppendorf, Hamburg, Germany

d M. Trepel  
Department of Oncology and Hematology, University Medical Center Hamburg-Eppendorf, Hamburg, Germany

Recent studies have shown that nanobodies allow higher tumor-to-background (T/B) ratios than conventional antibodies in molecular imaging applications *in vivo* (17,19). However, the T/B ratio depends on two parameters: specific binding of the antibody-construct leading to accumulation in the tumor as well as clearance of unbound constructs from the body. Both parameters depend on the molecular size of the probe. A small nanobody (~15 kDa) is expected to penetrate tumor tissue more rapidly than a larger conventional antibody (150 kDa). In turn, clearance of a nanobody via the kidney is fast, leading to short circulation times with a half-life of only ~1.5 h, as compared to days or weeks of conventional antibodies (3,11,21). Therefore, the comparison of two differently sized antibody-constructs for specific imaging of targets *in vivo* has to take into account the different kinetics of tumor accumulation and elimination from the circulation (11). This means that different imaging time points have to be investigated to determine best imaging conditions for each individual antibody construct. Moreover, different doses of the antibodies have to be compared, since higher doses may increase both specific and unspecific signals alike, thus reducing the maximum achievable T/B ratio.

There are only few studies directly comparing nanobodies and conventional antibodies for *in vivo* molecular imaging. Moreover, these studies did not optimize the doses of the conventional antibody and some used high doses of up to 100 µg antibody per animal (17,19). The high dosage inevitably leads to an excess of free circulating antibodies. When assessing T/B ratios based on the region of interest (ROI) in near-infrared fluorescence (NIRF) imaging experiments, the signal of the normal tissue serving as "background" will increase by the circulating antibodies. This results in lower T/B ratios of antibodies compared to nanobodies, not due to differences in specific signal, but due to higher unspecific background signal. Moreover, these excess antibodies are all prone to non-specific accumulation in target antigen-negative tumors by the enhanced permeability and retention (EPR) effect (22,23). Apart from kinetics and dosage, an intraindividual assessment of antigen-positive and -negative xenografts would enable a direct comparison of specific and unspecific signals due to the EPR effect. In addition, a comparative *ex vivo* analysis of explanted tumors would further determine the specificity observed in imaging experiments *in vivo* to optimize imaging conditions of differently sized constructs.

Therefore, we performed a direct NIRF-imaging comparison of a single-domain nanobody (*s+16a*, 17 kDa) and a monoclonal antibody (*Nika102*, 150 kDa) directed to the same target to improve specific *in vivo* NIRF-imaging in a lymphoma xenograft model. *S+16* is a nanobody (single variable domain) derived from a heavy-chain-only llama antibody. *Nika102* is a conventional monoclonal antibody (rat IgG2a kappa, composed of two heavy chains and two light chains) (Fig. 1A). Compared to mAb *Nika102*, nanobody *s+16a* exhibits a lower binding affinity (40 nM vs. 5 nM) and shorter *in vivo* blood half-life (2 h vs. 8 days) (11,24,25). The model target antigen ADP-ribosyltransferase ARTC2 is expressed on the surface of lymphoma cells (25–29). Beyond assessment of the advantages and disadvantages of nanobodies and conventional antibodies, this study was designed to determine the specific requirements, such as timing and dosage, for optimum imaging of tumors.

## 2. RESULTS

Purity of *s+16a* and *Nika102* before and after conjugation to AF680 was confirmed (Fig. 1B). Assessment of binding affinities

showed less than 10% reduction in labeling efficiencies upon overnight incubation in serum (Fig. 1C). Competition studies revealed that nanobody *s+16a* and antibody *Nika102* recognize different epitopes of ARTC2 (Fig. 1D). Internalization studies showed prominent staining of the cell surface upon incubation of cells at 4°C with both constructs. Upon incubation at 37°C, most of the labeled nanobody *s+16a*<sup>680</sup> and antibody *Nika102*<sup>680</sup> remained on the cell surface. Patchy cytosolic staining with both constructs after incubation for 24 h at 37°C indicates that a fraction of fluorescent label is internalized during prolonged incubation at 37°C (online Supplementary Fig. 1).

### 2.1. *In Vitro* NIRF-Imaging Experiments

Flow cytometry showed specific labeling of ARTC2-transfected DC27.10 lymphoma cells with *s+16a*<sup>680</sup> and *Nika102*<sup>680</sup>, but not of parental ARTC2-negative DC27.10 cells (Fig. 2A). Staining with *s+16a*<sup>680</sup> yielded lower fluorescence intensities (MFI = 15100 ± 1700) as compared to *Nika102*<sup>680</sup> (MFI = 73300 ± 1500), which reflects the lower labeling efficiency with fluorochrome AF680 of *s+16a* compared to *Nika102* (0.3 dyes/molecule for *s+16a* as compared to 2.0 dyes/molecule for *Nika102*). To provide a basis for the subsequent *in vivo* and *ex vivo* xenograft experiments, we further analyzed the same cells *in vitro* by fluorescence microscopy and with the NIRF-imaging system. Labeling of *s+16a* and *Nika102* with AF680 not only allowed detection of ARTC2-positive cells with fluorescence microscopy but also semi-quantitative analyses with the NIRF-imaging system intended for *in vivo* experiments (Fig. 2B, C). ARTC2-negative cells showed no detectable signals using either technique. As shown by flow cytometry, the fluorescence signal detected from ARTC2-positive cells with the NIRF-imaging system was lower when labeled with *s+16a*<sup>680</sup> (radiant efficiency =  $5.1 \pm 2.1 \times 10^7$ ) than with *Nika102*<sup>680</sup> (radiant efficiency =  $9.4 \pm 2.5 \times 10^7$ ). Signals from ARTC2-negative cells were more than 10 times lower than those of ARTC2-positive cells for *s+16a*<sup>680</sup> (radiant efficiency =  $3.0 \pm 1.5 \times 10^6$ ) as well as for *Nika102*<sup>680</sup> (radiant efficiency =  $3.5 \pm 2.3 \times 10^6$ ).

### 2.2. NIRF-Imaging Experiments *In Vivo*

Next, we aimed to evaluate the suitability of Alexa-680-conjugated nanobodies and antibodies for *in vivo* imaging of ARTC2-positive tumors. Therefore, we intravenously injected *s+16a*<sup>680</sup> and *Nika102*<sup>680</sup> into mice at four different doses (5, 10, 25, and 50 µg) 7–9 days after subcutaneous injection of ARTC2-positive and ARTC2-negative DC27.10 lymphoma cells on the opposite flanks of the same animals. The injected doses correspond to 0.004, 0.009, 0.022, and 0.044 mg of dye/kg for *s+16a*<sup>680</sup> and to 0.003, 0.006, 0.016, and 0.032 mg of dye/kg for *Nika102*<sup>680</sup> for a mouse of 24 g. Imaging was performed before and at defined time-points over 24 h after injection of the fluorochrome conjugates (Figs. 3 and 4 and Supplementary Fig. 1). The results showed efficient and specific labeling of ARTC2-positive tumors with both constructs. When injected with *Nika102*<sup>680</sup>, the specific signal in ARTC2-expressing tumors slowly increased over time, whereas after injection of *s+16a*<sup>680</sup>, the signal was already strong at early time points and declined over time (Fig. 3). Both constructs showed higher signals of ARTC2-positive tumors with increasing concentrations. At early time points after injection of *s+16a*<sup>680</sup>, strong signals were observed also in the kidneys, reflecting passage of the nanobodies through the renal filtration barrier. Note the high background signals of the entire animal

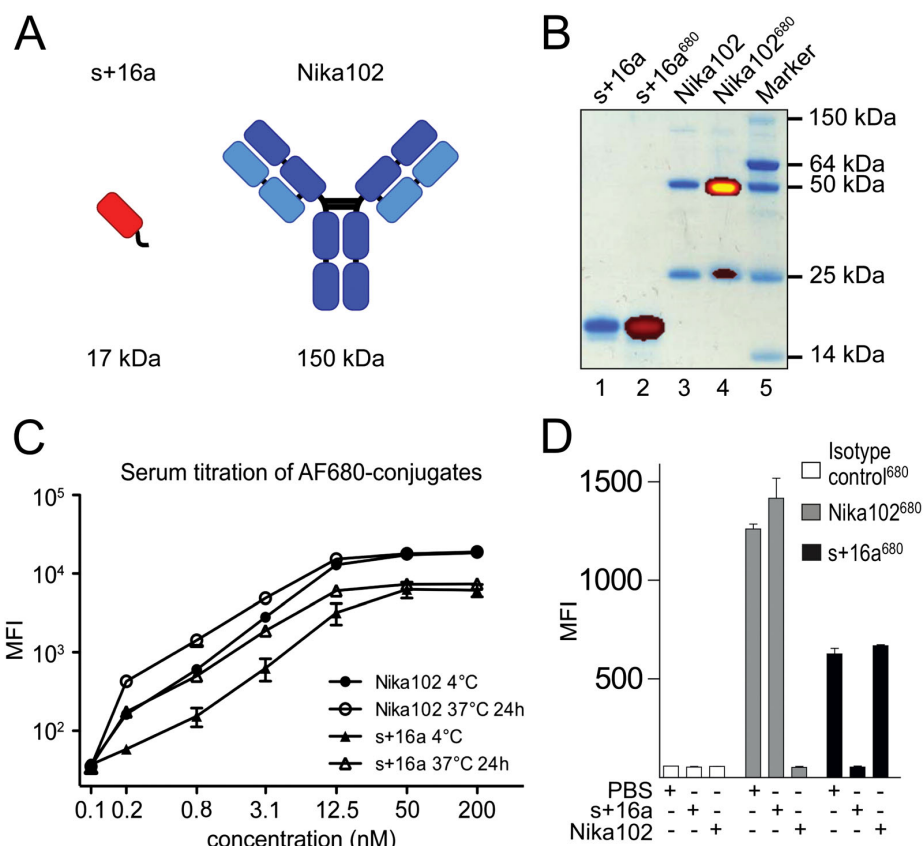


**Figure 1.** Structure, purity, stability and competition study of ARTC2-specific AF680-conjugates. (A) Scheme of nanobody s+16a and mAb Nika102. (B) Coomassie-stained gel overlaid by a corresponding NIRF image of unconjugated s+16a and Nika102 (lanes 1 and 3) and respective AF680-conjugates (lanes 2 and 4) (1 µg per lane of any given conjugate). (C) To assess the stability of the AF680-conjugates, conjugates were serially diluted and incubated for 24 h either at 4°C in PBS or at 37°C in serum. Conjugates were then used to stain ARTC2-expressing lymphoma cells before analysis by flow cytometry. Fluorescence intensities of the mean ± SD from three independent experiments are plotted. (D) ARTC2-expressing lymphoma cells were pretreated with PBS, unlabeled s+16a or Nika102 before staining with fluorochrome-conjugated Nika102, s+16a or isotype control antibodies and analysis by flow cytometry.

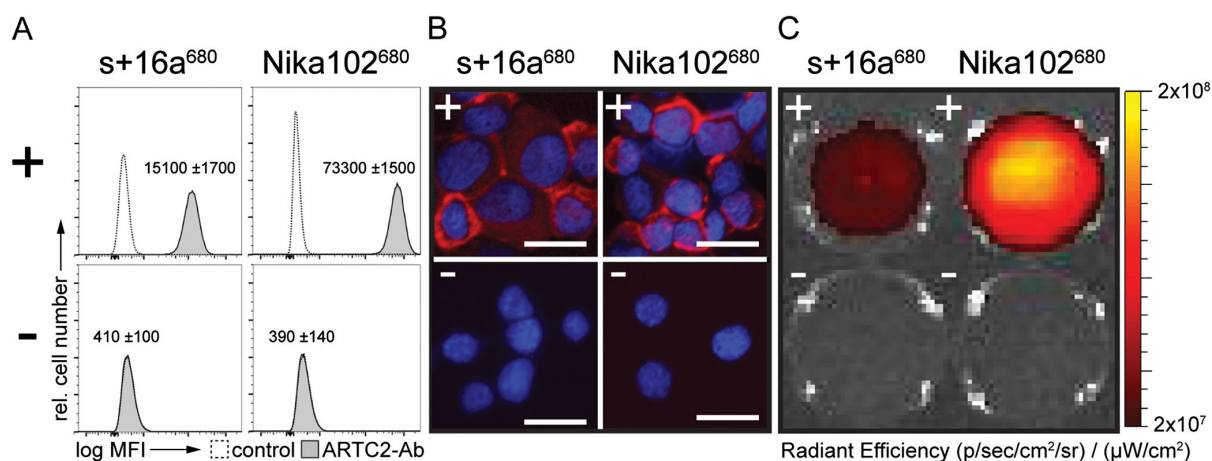


**Figure 2.** Imaging of AF680-conjugates *in vitro*. Untransfected (–) and ARTC2-transfected (+) DC27.10 lymphoma cells were incubated with s+16a<sup>680</sup> and Nika102<sup>680</sup>. (A) One aliquot of labeled cells (1 × 10<sup>5</sup>) was subjected to flow cytometry to quantify cell-bound AF680 conjugates. Mean fluorescence intensity of ARTC2 expression on lymphoma cells is plotted. Numbers indicate mean ± SD fluorescence intensity of ARTC2-positive cells (grey histograms) from three independent experiments. Unfilled histograms show isotype controls. (B) Another aliquot of labeled cells (1 × 10<sup>5</sup>) was used for fluorescence microscopic analysis of specific ARTC2 labeling (red). Nuclei were counter-stained with DAPI (blue). The size bar indicates 10 µm. (C) A third aliquot of cells (1 × 10<sup>7</sup>) was transferred onto a 96-well plate for NIRF imaging *in vitro*. Results are representative of three independent experiments.

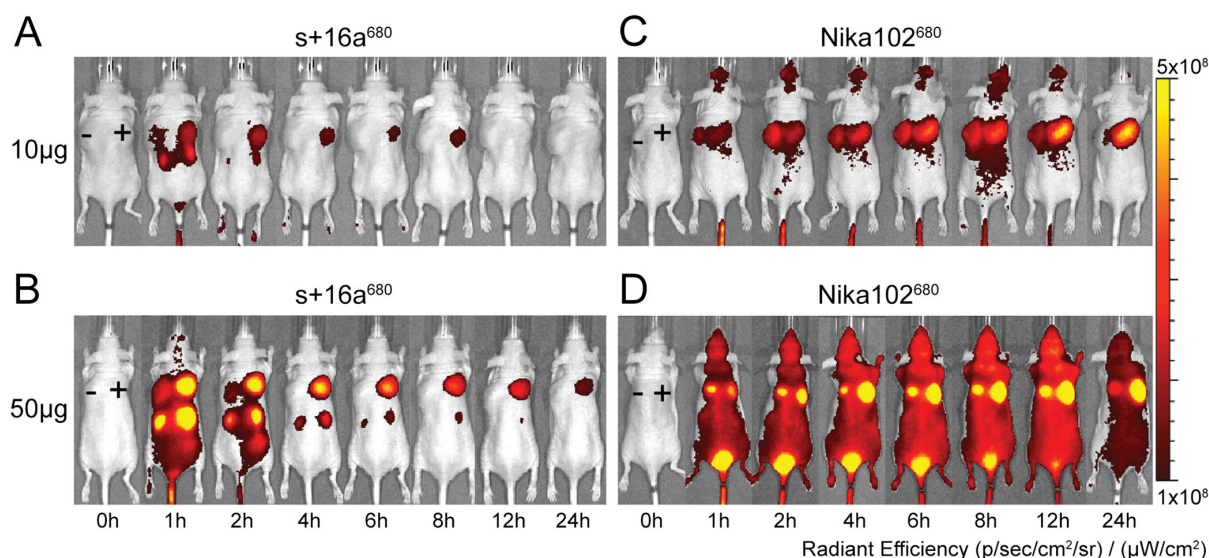


**Figure 3.** Comparison of different doses and time points for specific NIRF imaging *in vivo*. Seven to nine days after subcutaneous implantation of ARTC2-positive (+) and ARTC2-negative (-) lymphomas, s+16a<sup>680</sup> (A, B) and Nika102<sup>680</sup> (C, D) were injected intravenously at a dose of 10 µg (A, C) or 50 µg (B, D), respectively. NIRF imaging was performed before and 1, 2, 4, 6, 8, 12, and 24 h after injection. Signal intensities of all injected mice and imaging time points are all equally leveled to allow direct and fair visual comparison. Results are representative of at least three independent experiments. Levels of statistical significance are indicated by asterisks (\* =  $p < 0.05$ , \*\* =  $p < 0.01$ , \*\*\* =  $p < 0.001$ ).

after injection of 50 µg of Nika102<sup>680</sup> and the unspecific signals of the negative tumor when using higher doses of Nika102<sup>680</sup> (Figs. 3D and 4A).

The intermediate dose of 25 µg showed lower specific signals for both s+16a<sup>680</sup> and Nika102<sup>680</sup> as compared to 50 µg and higher specific signals as compared to 10 µg (Supplementary Fig. 2). The dose of 25 µg also showed higher unspecific signals in ARTC2-negative tumors for Nika102<sup>680</sup> resulting in a lower T/B-ratio as compared to 10 µg. The lowest dose of 5 µg showed the lowest specific and unspecific signals for both constructs with lowest resulting T/B ratios. In summary, the comparison of different doses of AF680-conjugates showed best imaging results with 50 µg of s+16a<sup>680</sup> and with 10 µg of Nika102<sup>680</sup> by achieving highest specific signal intensities (s+16a<sup>680</sup>) and by minimizing unspecific signals of ARTC2-negative tumors and background while maintaining sufficient specific signals (Nika102<sup>680</sup>), thereby allowing for highest T/B-ratios.

Semi-quantitative ROI analyses confirmed a rapidly increasing T/B ratio of ARTC2-positive tumors after injection of s+16a<sup>680</sup>, which reached a maximum of  $12.4 \pm 4.2$  (50 µg) and  $4.7 \pm 0.1$  (10 µg), respectively, already 4–6 h post-injection (Fig. 4B). The T/B ratio of ARTC2-positive tumors detected with s+16a<sup>680</sup> was significantly higher than of ARTC2-negative tumors throughout 2 h to 24 h post-injection. In contrast, the T/B ratio using Nika102<sup>680</sup> increased only slowly and reached its maximum of  $8.7 \pm 3.9$  (10 µg) and  $6.1 \pm 2.0$  (50 µg), respectively, not until 24 h post-injection. In the case of Nika102<sup>680</sup>, the T/B ratio of ARTC2-positive tumors was not significantly higher than of ARTC2-negative tumors until 8 h to 24 h post-injection due to the high unspecific signal of ARTC2-negative tumors.

The need to evaluate different time points and different doses when comparing differently sized antibodies for coherent NIRF-imaging experiments is illustrated in Fig. 5. The direct comparison of the T/B ratios obtained by using either 10 µg or 50 µg of each AF680-conjugate at different time points revealed that in

the case of s+16a<sup>680</sup>, significantly higher T/B ratios can be obtained with the higher concentration of 50 µg 4 to 6 h post-injection. Interestingly, in Nika102<sup>680</sup>-injected mice, a significant difference between the two dosing regimens was seen only after 24 h, and, as shown above, with a higher T/B ratio obtained by the lower concentration of 10 µg Nika102<sup>680</sup>. Based upon these observations, the following *ex vivo* experiments were performed at the optimum imaging time points and optimum probe concentrations of 6 h and 50 µg for s+16a<sup>680</sup> and of 24 h and 10 µg for Nika102<sup>680</sup>.

### 2.3. NIRF-Imaging Experiments Ex Vivo

ARTC2-positive and ARTC2-negative tumors were explanted 6 h and 24 h post-injection to quantify tumor-associated fluorescence and T/B ratios in the absence of potentially confounding signals from other tissues. The results of NIRF-imaging *ex vivo* reflect those of the *in vivo* experiments (Fig. 6). Both AF680 conjugates showed high signals from ARTC2-positive tumors, which decreased for s+16a<sup>680</sup> and increased for Nika102<sup>680</sup> over time (Fig. 6A). Signals of ARTC2-positive tumors were significantly higher than of ARTC2-negative tumors in the case of s+16a<sup>680</sup> only at 6 h ( $p < 0.001$ ) and in the case of Nika102<sup>680</sup> only at 24 h ( $p < 0.05$ ) post-injection. Note the low unspecific signal of ARTC2-negative tumors after injection of s+16a<sup>680</sup> at both time points, as compared to the high unspecific signal of ARTC2-negative tumors after injection of Nika102<sup>680</sup>. In the case of s+16a<sup>680</sup>, the T/B ratio of dissected ARTC2-positive tumors was significantly higher than that of ARTC2-negative tumors at both time points, 6 h and 24 h post injection ( $p < 0.01$  and  $p < 0.05$ , respectively) (Fig. 6B). As for the absolute signal intensities, Nika102<sup>680</sup> culminated in a significantly higher T/B ratio of positive tumors as compared to negative tumors only 24 h post-injection ( $p < 0.05$ ). Note the much higher T/B ratio ( $61.4 \pm 30.9$ ) of ARTC2-positive tumors 24 h post-injection of Nika102<sup>680</sup> as compared to the maximum achievable T/B ratio of s+16a<sup>680</sup>

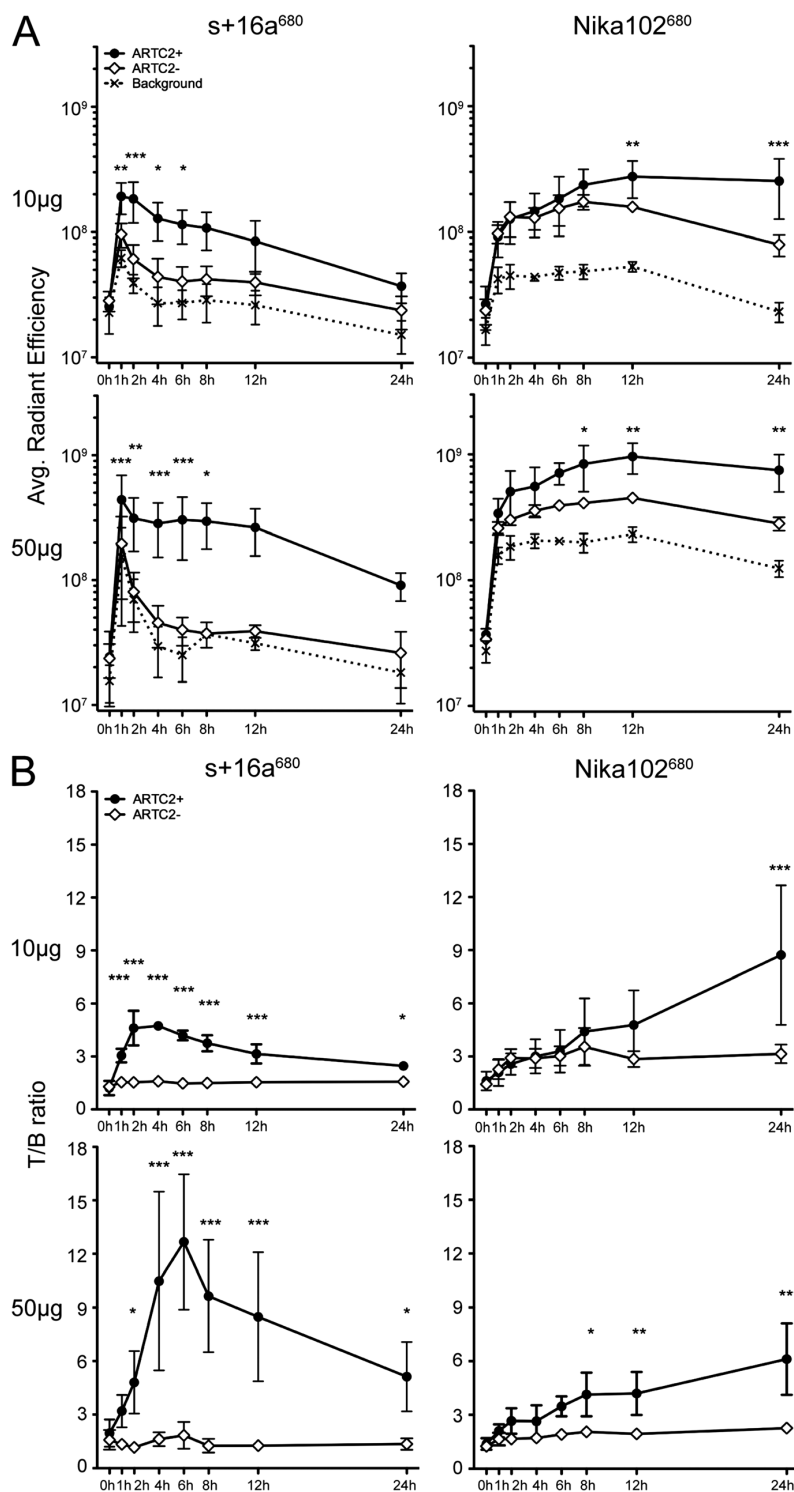


**Figure 4.** Radiant efficiency and T/B ratio of ARTC2-positive and ARTC2-negative tumors *in vivo*. S+16a<sup>680</sup> and Nika102<sup>680</sup> were injected into ARTC2-positive and ARTC2-negative tumor-bearing mice at a dose of 10 µg (upper panels) or 50 µg (lower panels), respectively. NIRF imaging was performed at different time points after injection and ROIs were drawn around tumors and normal tissue (hind leg) for semi-quantitative analyses. (A) Radiant efficiencies and (B) calculated T/B ratios of ARTC2-positive and ARTC2-negative tumors as well as background signals are plotted as a function of time. Data are presented as mean ± SD from at least three independent experiments for each group. Levels of statistical significance are indicated by asterisks (\* =  $p < 0.05$ , \*\* =  $p < 0.01$ , \*\*\* =  $p < 0.001$ ).

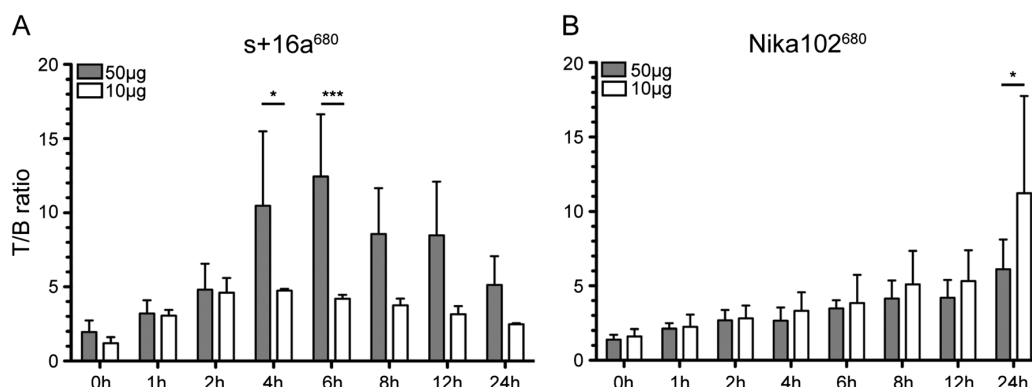


**Figure 5.** Optimization of probe concentration and NIRF-imaging time point for maximal T/B ratio of s+16a<sup>680</sup> and Nika102<sup>680</sup> *in vivo*. T/B ratios obtained from NIRF imaging of ARTC2-positive tumors are plotted as a function of time for mice injected with either 10 µg (white columns) or 50 µg (grey columns) of (A) s+16a<sup>680</sup> and (B) Nika102<sup>680</sup>, respectively. Fifty micrograms of s+16a<sup>680</sup> showed a higher T/B ratio than 10 µg, which was significant 4–6 h post-injection. Nika102<sup>680</sup> showed the opposite behavior, the lower dose yielded a higher T/B ratio than the higher dose, which became significant after 24 h. Data are presented as mean ± SD from three to seven independent experiments. Levels of statistical significance are indicated by asterisks (ns =  $p > 0.05$ , \* =  $p < 0.05$ , \*\* =  $p < 0.01$ , \*\*\* =  $p < 0.001$ ).

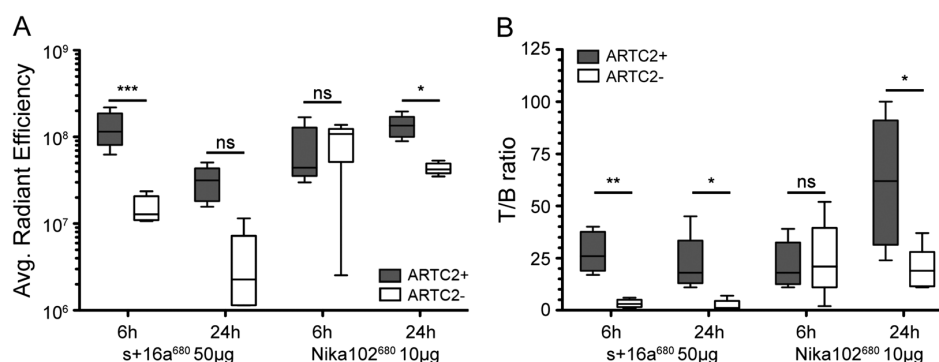


**Figure 6.** NIRF imaging *ex vivo*. ARTC2-positive (+) and ARTC2-negative (–) tumors of mice injected with 50 µg s+16a<sup>680</sup> or with 10 µg Nika102<sup>680</sup> were explanted 6 h and 24 h post-injection in order to quantitate tumor-associated fluorescence and T/B ratios using NIRF imaging in the absence of potentially confounding signals from other tissues. (A) Radiant efficiencies of tumors and (B) T/B ratios are presented as mean ± SD from five independent experiments.

(27.8 ± 9.6) after 6 h in the absence of confounding signals from normal tissue.

Biodistribution analyses of spleen, lungs, liver, kidneys, stomach, ileum, and muscle revealed an overall decline of signal intensities at 24 h as compared to 6 h (Fig. 7A). At both time points, 6 h and 24 h post-injection, the highest unspecific organ-to-background ratios were observed for the liver in the case of Nika102<sup>680</sup> and for the kidneys in the case of s+16a<sup>680</sup> (Fig. 7B). Interestingly, in the case of Nika102<sup>680</sup>, at 6 h post-injection the second highest organ-to-background ratio was observed for the ARTC2-negative tumor and at 24 h the ARTC2-negative tumor showed even the highest unspecific signals when compared to other organs.

#### 2.4. Flow Cytometry and Fluorescence Microscopy *Ex Vivo*

Next, we determined possible causes of the unspecific signals from normal tissue after injection of Nika102<sup>680</sup> *in vivo* (Figs. 3D, 4A) as well as from ARTC2-negative tumors *in vivo* and *ex vivo* (Figs. 4A and 6). Therefore, we performed flow cytometry *ex vivo* to quantify levels of unbound AF680-conjugates in serum and of

cell bound AF680-conjugates on dispersed cells from the explanted tumors (Fig. 8). Serum samples showed little, if any, detectable circulating s+16a<sup>680</sup> at 6 h and 24 h post-injection (Fig. 8A). In contrast, mice that had been injected with Nika102<sup>680</sup> showed significantly higher levels of unbound circulating Nika102<sup>680</sup> in serum at both time points, which somewhat decreased over time, but were still present in excess 24 h post-injection. Urine analyses revealed high levels of s+16a<sup>680</sup>, particularly 6 h post-injection, but little, if any, Nika102<sup>680</sup> (data not shown).

Flow cytometry of dispersed cells from xenografts dissected 6 h and 24 h post-injection showed specific labeling of ARTC2-positive lymphoma cells with both AF680-conjugates and no unspecific labeling of ARTC2-negative tumor cells (Fig. 8B). As seen with NIRF-imaging *in vivo* and *ex vivo*, labeling and specific signals from ARTC2-positive tumors decreased over time after injection of s+16a<sup>680</sup>, whereas signals of ARTC2-positive tumors from animals injected with Nika102<sup>680</sup> increased over time. Signals of cells from ARTC2-positive tumors from animals injected with s+16a<sup>680</sup> were higher than signals after injection of Nika102<sup>680</sup> at 6 h post injection, but lower at 24 h after injection.

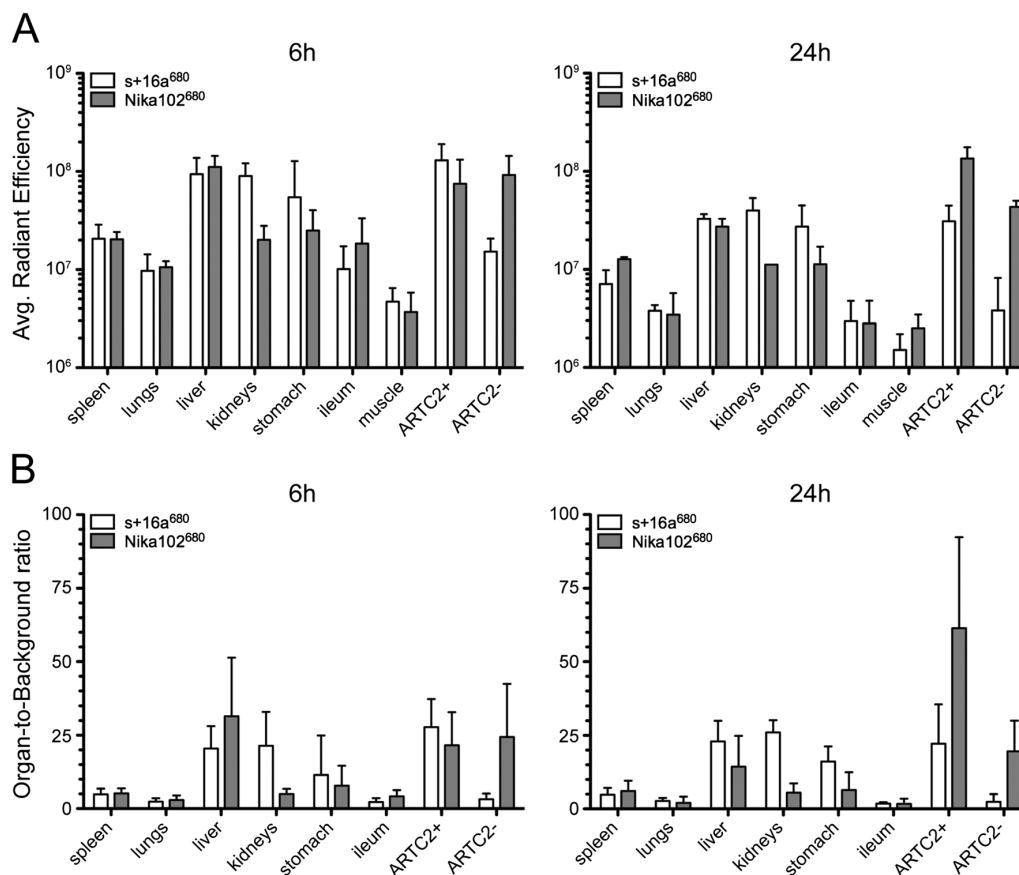


**Figure 7.** Biodistribution analyses. At 6 h and 24 h post-injection of 50  $\mu\text{g}$  s+16a<sup>680</sup> or 10  $\mu\text{g}$  Nika102<sup>680</sup> mice were sacrificed and tumors and organs were explanted. (A) Organ- and tumor-associated fluorescence was quantified and (B) organ- and tumor-to-background ratios were calculated using NIRF imaging in the absence of confounding signals from other tissues. Signals from explanted muscle tissue served as background value to calculate ratios. Radiant efficiencies of organs and tumors and organ- and tumor-to-background ratios are presented as mean  $\pm$  SD from five independent experiments.

We further analyzed the distribution of injected AF680-conjugates within explanted and cryosectioned tumors *ex vivo* by confocal fluorescence microscopy (Fig. 9). S+16a<sup>680</sup> revealed homogeneous and specific labeling of ARTC2-positive tumor cells 6 h post-injection, similar to the staining of these cells in culture (Fig. 2B). In contrast, Nika102<sup>680</sup> showed only weak staining of cells in ARTC2-positive tumors after 6 h. Moreover, the monoclonal antibody showed staining evidently not associated with tumor cells in both ARTC2-positive and ARTC2-negative tumors (Fig. 9A, arrow).

### 3. DISCUSSION

The utility for both nanobodies and conventional antibodies for *in vivo* imaging is well established, but optimum dosing and timing schedules for one versus the other have not been determined so far. Here, we used NIRF-dye AF680-conjugated nanobodies and conventional monoclonal antibodies directed at the same target on lymphoma cells for a direct comparison of *in vivo* and *ex vivo* analyses. We showed that nanobodies are well suited as diagnostic tools for rapid and specific *in vivo* detection of lymphomas, with superior tissue penetration compared to conventional antibodies and significantly higher T/B ratios

when performing same-day imaging *in vivo*. In addition, our experiments revealed that at later time points the T/B ratio of conventional antibodies can be improved by using lower doses of antibody conjugates.

*In vitro*, both, nanobody s+16a<sup>680</sup> and antibody Nika102<sup>680</sup> bound specifically to ARTC2-positive lymphoma cells with no unspecific labeling of ARTC2-negative cells (Fig. 2). Albeit that Nika102<sup>680</sup> showed stronger signals *in vitro*, s+16a<sup>680</sup> allowed a faster and more specific detection of ARTC2-positive xenografts *in vivo* (Figs. 3 and 4). Apart from the different kinetics for best tumor visualization *in vivo*, the major drawback of Nika102<sup>680</sup> at higher doses (50  $\mu\text{g}$ ) was the high unspecific signal originating not only from normal tissues (causing fluorescence signals from the entire mouse), but also from ARTC2-negative tumors (Fig. 4). This apparently insufficient T/B ratio could be improved by using a lower dose (10  $\mu\text{g}$ ) of Nika102<sup>680</sup>, resulting in dramatically reduced signals of normal tissues and ARTC2-negative tumors and only slightly decreased specific signals of ARTC2-positive tumors (Fig. 5). In contrast, increasing the dose of s+16a<sup>680</sup> caused stronger signals of ARTC2-positive tumors but not of normal tissue or ARTC2-negative tumors.

NIRF imaging of dissected tumors *ex vivo* revealed the overall strongest T/B ratio of ARTC2-positive tumors 24 h post-injection

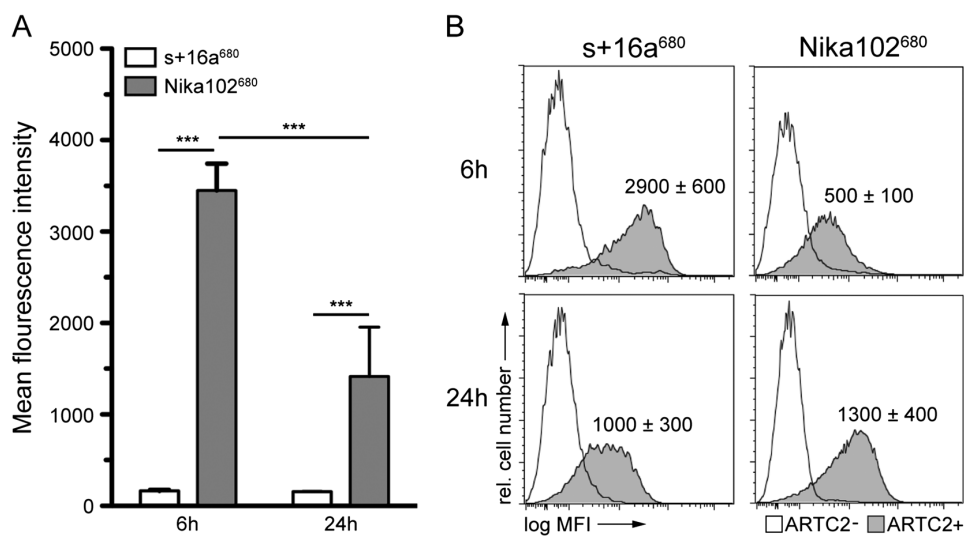


**Figure 8.** Flow cytometric analyses of circulating and cell bound s+16a<sup>680</sup> and Nika102<sup>680</sup>. (A) In order to determine a cause for the high background signals and the unspecific signal of ARTC2-negative tumors post-injection of Nika102<sup>680</sup>, we analyzed serum to monitor levels of circulating unbound AF680-conjugates. Mice bearing ARTC2-negative and ARTC2-positive tumors were injected intravenously with 50 μg s+16a<sup>680</sup> and 10 μg Nika102<sup>680</sup> and sacrificed 6 h and 24 h after injection. Serum at a dilution of 1:100 was used to label ARTC2-transfected lymphoma cells for flow cytometric quantification of circulating intact AF680 conjugates. Fluorescence intensities of the mean ± SD from three independent experiments are plotted. Levels of statistical significance are indicated by asterisks (\*\*\* =  $p < 0.001$ ). (B) To determine the level of injected conjugates specifically bound to tumor cells both ARTC2-positive and ARTC2-negative tumors were dissected from the same animals. Single-cell suspensions were counterstained with anti-CD45 and analyzed by flow cytometry to quantify the amount of cell-bound AF680 conjugates. Means and standard deviations of fluorescence intensities (MFI) from three independent experiments are plotted.

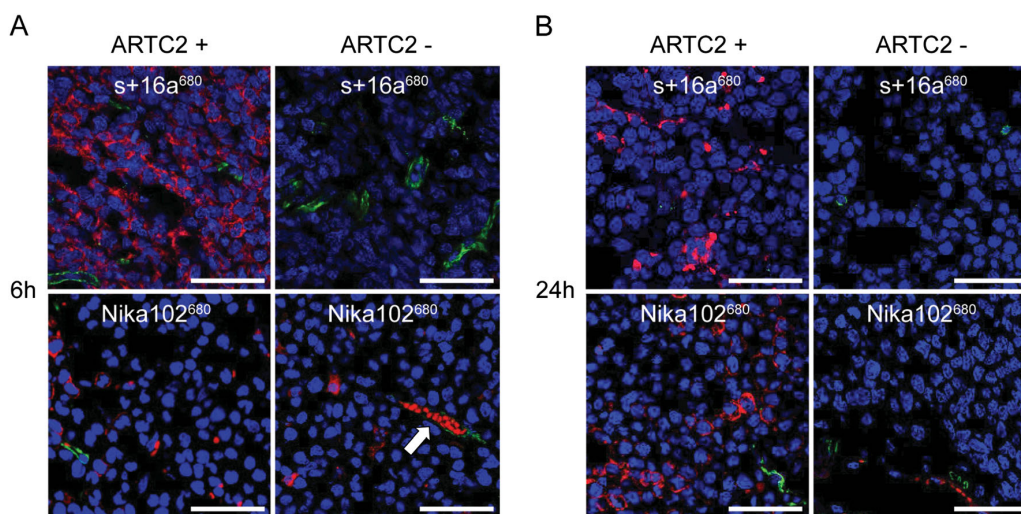


**Figure 9.** Fluorescence microscopy *ex vivo* of ARTC2-positive and ARTC2-negative tumors. Confocal fluorescence microscopy (40×) of tumor cryosections (A) 6 h and (B) 24 h post-injection of 50 μg s+16a<sup>680</sup> and 10 μg Nika102<sup>680</sup>, respectively. Signal intensities of AF680-conjugates are displayed in red and demonstrate the distribution within the tumor 6 h and 24 h after injection. Nuclei were counter-stained *ex vivo* with DAPI (blue) and blood vessels were stained with anti-CD31<sup>488</sup> (green). Nanobody s+16a<sup>680</sup> revealed homogeneous and specific labeling of ARTC2-positive tumors readily within 6 h, whereas Nika102<sup>680</sup> showed weak staining after 6 h, which increased only after 24 h. At both imaging time points Nika102<sup>680</sup> also showed unspecific staining within or close to the tumor vasculature (arrow) of both ARTC2-negative and positive tumors. The size bar indicates 50 μm. These results are representative of three independent experiments.

of Nika102<sup>680</sup> in the absence of potentially confounding signals from other tissues (Fig. 5). These *in vivo* and *ex vivo* NIRF-imaging observations could be well explained by the results of *ex vivo* flow cytometric analyses for quantification of injected AF680-

conjugates in serum (Fig. 8A). These showed high levels of unbound and free circulating Nika102<sup>680</sup> 6 h and even 24 h post-injection, even at the lower dose of 10 μg, whereas after the injection of 50 μg of s+16a<sup>680</sup> no unbound nanobodies were

detectable in serum at these time points. These results are in accordance with a recent study in which we determined the pharmacokinetics of s+16a<sup>680</sup> and Nika102<sup>680</sup> (11). It is conceivable, that higher doses would further increase the amount of free circulating Nika102<sup>680</sup>, and thereby further increase the observed unspecific signals *in vivo*. *Ex vivo* flow cytometric analyses of dispersed cells from dissected tumors showed specific staining of ARTC2-positive tumor cells with both constructs but no unspecific binding of injected AF680-conjugates to ARTC2-negative lymphoma cells (Fig. 8B). These findings are consistent with *in vitro* labeling experiments, which show prominent cell-surface staining of ART2-positive tumor cells as well as some internalized fluorescence for both constructs after 24 h incubation at 37°C (Supplementary Fig. 1). The higher staining intensity of ART2-positive tumor cells with nanobody s+16a<sup>680</sup> than with mAb Nika102<sup>680</sup> at 6 h post-injection likely reflects the higher injected dose and faster tissue penetration of the nanobody. The lower staining intensity of ART2-positive tumor cells with nanobody s+16a<sup>680</sup> than with mAb Nika102<sup>680</sup> at 24 h post-injection likely reflects the lower affinity and renal elimination of excess nanobody. The increase in staining intensity of mAb Nika102<sup>680</sup> at 24 h versus 6 h likely reflects increasing accumulation in the tumor from excess levels of circulating mAb. Fluorescence microscopy completed the *ex vivo* imaging approach. In the case of the nanobody s+16a, homogeneous staining of cells in ART2C-positive tumor sections correlated well with the staining of cells *in vitro* (Figs. 9A and 2B), confirming that the nanobody was able to reach even remote areas within the tumor after 6 h. In contrast, the monoclonal antibody showed only weak staining of cells in ARTC2-positive tumors after 6 h. Moreover, the monoclonal antibody showed staining within or close to the tumor vasculature even in ARTC2-negative tumors (Fig. 9A), providing a plausible explanation for the unspecific signals during *in vivo* imaging. The better tissue penetration of the nanobody s+16a at early time points is likely attributed to its ability to cross the endothelial barrier more easily to reach its target.

NIRF imaging of other organs *ex vivo* revealed high unspecific signals for the liver in the case of Nika102<sup>680</sup> and for kidneys in the case of s+16a<sup>680</sup>. High signals in the kidney at early time points are consistent with renal filtration and partial retention of nanobody s+16a<sup>680</sup> in the kidneys. High signals in the liver for both constructs are consistent with hepatic elimination of fluorochromes. Note that at the time point of *ex vivo* analyses (6 h and 24 h), the signals from kidneys had already decreased dramatically as compared to the *in vivo* signals at 1 h and 2 h post-injection, presumably by elimination of most of labeled nanobody s+16a<sup>680</sup> from the body via urination. Signals from the kidneys even after 24 h likely reflect partial tubular resorption of nanobodies and/or fluorochromes.

As in previous studies, the results reported here emphasize that molecular imaging with labeled nanobodies *in vivo* allows rapid and specific same-day tumor imaging, including the possibility of increasing the dose for optimized T/B ratios without compromising specificity of marked tissues (12–15,17–19). Our study also reveals, that *in vivo* molecular imaging using conventional antibodies can be considerably improved by determining the optimum dose of the injected large (and therefore not renally cleared) antibodies. A fivefold lower dose of conventional antibody can almost double the T/B ratio. Recent studies, comparing nanobodies and conventional antibodies for *in vivo* molecular imaging neglected to optimize the dose of the

investigated conventional antibody and used very high doses of up to 100 µg per animal (17,19). This leads to an excess of free-circulating antibodies, as we were able to show for mAb Nika102<sup>680</sup> in the present study. These excess antibodies are prone to nonspecific accumulation in target-negative tumors by the enhanced permeability and retention effect (EPR) described earlier for conventional antibodies (22,23). It should be noted, that the EPR effect also leads to an increased uptake of antibodies in the target-positive tumors and may thereby contribute to increase the specific signals at low antibody doses. Taken together, thorough dose optimization of conventional antibodies should be performed for *in vivo* imaging applications.

For nanobodies, in contrast, dose optimization seems to be less of an issue, since any excess is renally cleared within 2 h and thus unspecific accumulation in non-targeted tissue is minimized. This allows same-day imaging and could be translatable to the clinical setting. However, next-day imaging might be more convenient in a clinical setting. Further, the cost efficiency might be better for the antibody due to the lower dose required, even though nanobodies can be produced at low costs in bacteria and yeast (10).

A limitation of our study is that we did not optimize the amount of fluorescent dyes per antibody construct, which might affect the maximum achievable signal for imaging. Another improvement of the labeling strategy would have been the site-specific conjugation of the NIRF dye, as recently described by Kijanka *et al.*, instead of random conjugation to primary amine groups, which might affect binding affinity (17). Another limitation is that we injected fixed doses of 5, 10, 25 and 50 µg of our constructs regardless of the weight of the animals, instead of performing weight-adapted injections. The differences in weight of individual mice (range 22.5–26.1 g) may explain some of the observed signal variations within different dose groups.

The region chosen for “background” signal estimation also influences the calculated T/B ratios. However, nanobody s+16a and mAb Nika102 show different accumulations in different abdominal organs and blood, precluding a fair and comparable estimation of T/B ratios with these tissues. As an alternative, we chose the hind limb and muscle, respectively, because this tissue introduced less variation, even though it might underestimate the systemic background.

In addition, further studies should investigate time points later than 24 h post-injection (e.g. 48 h, 72 h). These might show a further improvement of the maximum achievable T/B ratio using the conventional antibody, as recently shown for Trastuzumab by Kijanka *et al.* (17). A limitation of nanobodies in imaging is the high confounding signal of the kidneys due to their renal elimination, which is particularly prominent at early time points. This confounding signal might limit the ability of nanobodies to detect tumors located close to the kidneys. However, the renal retention of nanobodies can be reduced by 45% upon co-injection of gelofusine and lysine without reduced tumor uptake, as reported by Gainkam *et al.* (30).

An intrinsic limitation when comparing llama-derived nanobodies and conventional antibodies is the fact that they bind to different epitopes of the target antigen, which might influence antibody internalization, unspecific binding to other sites or uptake by the reticular endothelial system, thereby affecting blood half-life. However, the differences observed here in terms of dose and timing for optimal imaging can be mainly explained by the size difference of the nanobody and the conventional antibody.

An inherent technical limitation of NIRF imaging is its low penetration depth of 7–10 mm, which is particularly suited for imaging of subcutaneous tumors but does not allow for imaging of orthotopic tumors. However, even for subcutaneous tumors, some spillover from abdominal organs such as kidneys or liver cannot be excluded. Therefore, thorough *ex vivo* validation experiments of explanted tumors and organs are mandatory. Another limitation of NIRF imaging is the only semi-quantitative assessment of biodistribution as compared to radionuclide-mediated imaging. However, this limitation is compensated in part by the suitability of NIRF-labeled probes for *ex vivo* validation experiments, that is, quantitative flow cytometric assessment of antibodies bound to tumor cells. Moreover, for the principle aim of this study, that is, optimizing timing and dosing of nanobodies and antibodies for imaging *in vivo*, the NIRF technique is well suited. Our results are in accord with a recent study by Oliveira *et al.* using NIRF-labeled nanobodies (19). If desired, nanobodies can also be radiolabeled for positron emission tomography (PET) imaging of xenograft models. A recent study that compared nanobodies and conventional antibodies for PET imaging also came to the conclusion that nanobodies allow same-day imaging with high tumor-to-background ratios (15).

## 4. CONCLUSIONS

Labeling of nanobody s+16a and antibody Nika102 with AF680 allowed validation of *in vivo* NIRF-imaging results with *ex vivo* flow-cytometry and fluorescence-microscopy. For this reason, and because it is nonradioactive, highly sensitive, inexpensive, and uses comparatively easy-to-produce targeted probes, we advocate the use of the NIRF-imaging technique for evaluation of new antibody constructs in preclinical molecular imaging experiments.

Our comparative *in vivo* and *ex vivo* analyses revealed that the specific contrast between tumor and normal tissue is more important than the absolute amount of conjugate that reaches the tumor. Moreover, our study confirmed that timing and dosage significantly influence specific and unspecific *in vivo* NIRF-imaging signals of s+16a<sup>680</sup> and Nika102<sup>680</sup>. Nanobody s+16a allowed same-day imaging with high tumor-to-background ratio, whereas antibody Nika102 gave optimal imaging results only 24 h post-injection. Nanobody s+16 required a high dose while antibody Nika102 had the best tumor-to-background ratio at a low dose. Therefore, timing and dosage should be addressed when using nanobodies and conventional antibodies for molecular imaging purposes.

## 5. EXPERIMENTAL

### 5.1. Cell Lines and Mice

ARTC2-transfected and untransfected DC27.10 murine lymphoma cells were cultured as described previously (26). The closely related ARTC2.1 and ARTC2.2T cell GPI-anchored cell surface ecto-enzymes are encoded by tandem genes. The study was performed with reagents specific for ARTC2.2, for better legibility we use the term ARTC2. Tumor xenograft experiments were conducted using athymic nude mice (NMRI-Foxn1<sup>nu</sup>) weighting 24.0 ± 1.4 g (range 22.5 to 26.1 g). Mice were obtained from Charles River Laboratories (Sulzfeld, Germany). Experiments were performed in accordance with international guidelines on the ethical use of animals and were approved by the local animal welfare commission.

### 5.2. Generation of AF680-Conjugates

Generation and purification of ARTC2.2-specific nanobody s+16a (~17 kDa) and of monoclonal antibody Nika102 (150 kDa) were described previously (24,25). S+16a carries C-terminal His6x and c-Myc epitope tags and has a calculated size of 17.4 kDa (25). Nanobody s+16a and antibody Nika102 were conjugated to the fluorescent dye AlexaFluor-680 (AF680) (Molecular Probes, Carlsbad, CA, USA) (excitation wavelength = 679 nm, emission wavelength = 702 nm) and number of dye molecules per probe were calculated using molar extinction coefficients of 15720 cm<sup>-1</sup>M<sup>-1</sup> and 203000 cm<sup>-1</sup>M<sup>-1</sup>, respectively. Purity of antibody constructs before and after conjugation to AF680 was assessed by SDS-PAGE size fractionation and Coomassie brilliant blue gel stain as described previously (11). Binding affinities as well as stability during overnight incubation at 37°C in serum were assessed by serial dilution of probes and flow cytometric analyses of labeled DC27.10 cells. Competition studies were performed to evaluate whether s+16a and Nika102 recognize distinct or overlapping epitopes. ARTC2-transfected DC27.10 cells were pretreated with phosphate buffered saline (PBS), unlabeled s+16a (5 µg/100 µL) or unlabeled Nika102 (5 µg/100 µL) for 20 min at 4°C before exposure to AF680-conjugated Nika102 (0.2 µg/100 µL), s+16a (0.2 µg/100 µL) or isotype control antibodies for 20 min and analysed by flow cytometry. Internalization studies were performed by staining of DC27.10 ARTC2 cells with s+16a<sup>680</sup> Nika102<sup>680</sup> for 30 min on ice and washed. Cells were further incubated in cell culture medium at 4°C for 2 h or at 37°C for 2 and 24 h before fixation in 2% PFA, counterstaining with Hoechst 33428, and analysis by fluorescence microscopy.

### 5.3. In Vitro Analyses

For *in vitro* flow-cytometric analyses, 1 × 10<sup>6</sup> untransfected or ARTC2-transfected DC27.10 cells were stained with s+16a<sup>680</sup> or Nika102<sup>680</sup> (1 µg/µL) or control antibodies for 30 min at 4°C. Cells were washed twice and analyzed by flow cytometry on a FACS Canto II (BD Biosciences, Becton Dickinson, Franklin Lakes, USA). Dead cells were excluded after staining with propidium iodide. Flow cytometry data was analyzed with FlowJo 9.3 software (Tree Star Inc, Ashland, OR, USA).

For *in vitro* fluorescence microscopy, 1 × 10<sup>5</sup> untransfected or ARTC2-transfected DC27.10 cells were stained with either s+16a<sup>680</sup>, Nika102<sup>680</sup> or control antibodies as described above. Cells were suspended in a volume of 0.2 mL of PBS and centrifuged (CytoSpin, Shandon, Pittsburgh, PA, USA) onto microscope slides at 800 rpm for 5 min. Cells were fixed in acetone for 10 min, washed twice in PBS, and mounted with Mowiol-DAPI (Molecular Probes, Carlsbad, CA, USA). After air-drying for 24 h, slides were analysed with an inverted microscope (Axiovert 200 m, Zeiss, Goettingen, Germany) with excitation of 665 nm and emission of 725 nm. Images were analyzed with ImageJ software (NIH, Bethesda, Maryland, USA).

For NIRF imaging *in vitro*, 1 × 10<sup>7</sup> untransfected or ARTC2-transfected DC27.10 cells were stained with either, s+16a<sup>680</sup>, Nika102<sup>680</sup> or control antibodies as described above. Cells were sedimented on a black 96-well plate (Nunc, Waltham, Massachusetts, USA). Measurements were performed with a small-animal NIRF-imaging system (IVIS-200, Caliper Life Sciences, Hopkinton, Massachusetts, USA) using fluorescent filter sets of 515–665 nm for excitation, 695–770 nm for emission, and 580–610 nm for background subtraction with a 512 × 512-pixel matrix size

( $15 \times 15 \mu\text{m}/\text{pixel}$ ). Images were analysed semi-quantitatively by placing a region of interest (ROI) on individual wells. Total radiant efficiency was calculated with Living Image 4.2 software (Caliper Life Sciences).

#### 5.4. NIRF Imaging *In Vivo*

Prior to NIRF imaging *in vivo*, 8–10-week-old mice were kept on an alfalfa-free diet for 7 days to reduce autofluorescence of the intestine. For generation of tumor xenografts of comparable size, mice were subcutaneously injected at their back on the right side with  $1.5 \times 10^6$  ARTC2-transfected cells and on the left side with  $0.5 \times 10^6$  untransfected cells in a mix of 0.1 mL RPMI medium and 0.1 mL Matrigel (BD Biosciences, Becton Dickinson, Franklin Lakes, USA). The different number of cells has been used to take into account the different growth rates of transfected and untransfected cells. After 7–9 days, when tumors reached ~8 mm in diameter, nanobody s+16a<sup>680</sup> or conventional antibody Nika102<sup>680</sup> was injected intravenously via the tail vein in a volume of 200  $\mu\text{L}$ . NIRF imaging was performed before injection and 1, 2, 4, 6, 8, 12, and 24 h after injection. Initial studies showed that earlier time points did not yield useful diagnostic information due to high unspecific signals and were therefore not assessed. Experiments were performed with four doses of each AF680-conjugate: 5  $\mu\text{g}$ , 10  $\mu\text{g}$ , 25  $\mu\text{g}$ , and 50  $\mu\text{g}$ . This corresponded to 0.1  $\mu\text{g}$ , 0.2  $\mu\text{g}$ , 0.45  $\mu\text{g}$  and 0.9  $\mu\text{g}$  of injected dye for nanobody s+16a and 0.06  $\mu\text{g}$ , 0.12  $\mu\text{g}$ , 0.3  $\mu\text{g}$ , and 0.6  $\mu\text{g}$  of injected dye for monoclonal antibody Nika102.

For NIRF imaging *in vivo*, mice were anesthetized with isoflurane and positioned in the imaging chamber of the small-animal NIRF-imaging system using the same filter settings as described above. After qualitative imaging *in vivo*, quantitative analyses were performed by placing ROIs around the ARTC2-positive tumors, the ARTC2-negative tumors (negative control) and the hind limb (background signal). Even though the signal of the hind limb might underestimate the systemic background, we chose the hind limb because this tissue introduces less variation than abdominal organs or blood.

Total radiant efficiency was determined with Living Image 4.2 software (Caliper Life Sciences). Tumor-to-background ratio was calculated by dividing the tumor uptake value by the background value determined from the hind limb.

#### 5.5. Ex Vivo Analyses

For *ex vivo* validation of *in vivo* measurements, animals were sacrificed 6 h or 24 h post-injection. ARTC2-positive and ARTC2-negative tumors and organs (spleen, lungs, liver, kidneys, stomach, ileum and muscle) were dissected. Biodistribution analysis was performed using NIRF imaging *ex vivo* as described by Bannas *et al.* (11). Total radiant efficiency of organs and tumors was determined and organ- and tumor-to-background ratio was calculated by dividing the tumor uptake value by the background value determined from explanted muscle tissue. Even though the signal of muscle might underestimate the systemic background, we chose muscle because this tissue introduces less variation than abdominal organs or blood.

For *ex vivo* fluorescence microscopy, one half of each harvested tumor was fixed in 4% paraformaldehyde over night, placed in 30% sucrose for 24 h and frozen on dry ice in Tissue-Tek<sup>®</sup> OCT™ (Sakura Finetek, Alphen, The Netherlands). Sections of 8  $\mu\text{m}$  were prepared using a Reichert-Jung Ultracut microtome

(Reichert-Jung, Wien, Austria). Tumor cryosections were stained with DAPI (Molecular Probes, Carlsbad, CA, USA) to visualize nuclei and CD31 (M-20, Santa Cruz, Heidelberg, Germany) to visualize vessels. Fluorescence microscopy analysis was performed using a Leica TCS SP5 confocal microscope (Leica Camera AG, Solms, Germany). A HeNe 633 nm laser was used for excitation of AlexaFluor680. Image analysis was performed using Leica LAS (Leica) and ImageJ software (NIH, USA).

For flow cytometry *ex vivo*, the other half of each tumor was dissected and passed through a 70  $\mu\text{m}$  cell strainer to obtain single-cell suspensions. Dispersed cells were counterstained with pan leukocyte marker anti-CD45 (Clone 30-F1, eBioscience, San Diego, CA, USA) and Pacific Orange-NHS dye (Invitrogen, Grand Island, NY, USA) for live/dead staining. Labeling efficiency of ARTC2 by the injected AF680-conjugates was quantified by flow cytometry. For quantification of free circulating AF680-conjugates, serum was collected and used in a volume of 100  $\mu\text{L}$  (1:100 dilution) for labeling  $1 \times 10^6$  ARTC2-expressing DC27.10 cells with subsequent flow cytometry.

#### 5.6. Statistical Analysis

Data are presented as mean  $\pm$  SD. Statistical analysis was performed using two-way ANOVA with Bonferroni's post-test analyses to evaluate differences between the two independent variables from experiments presented in Figs. 4 and 5. One-way ANOVA with Bonferroni's post-test analyses was performed to evaluate the significance of differences between four groups shown in Figs. 6 and 7A.  $P < 0.05$  indicates statistical significance. Statistical analysis was performed using Prism 5, Graph Pad Software and Excel, Microsoft.

### Acknowledgements

Parts of this work represent partial fulfillment of the requirements for the graduate thesis of Alexander Lenz at the University Hospital, Hamburg. This work was supported by the graduate school 'Inflammation and regeneration' of the Collaborative Research Centre 841 of the Deutsche Forschungsgemeinschaft (Alexander Lenz, Valentin Kunick), by the Collaborative Research Centre 877 of the Deutsche Forschungsgemeinschaft (Friedrich Koch-Nolte), by the Werner Otto Foundation (Peter Bannas), by the Wilhelm Sander Foundation (Peter Bannas, Friedrich Koch-Nolte), and by the Deutsche Forschungsgemeinschaft (Martin Trepel, Friedrich Haag and Friedrich Koch-Nolte).

### REFERENCES

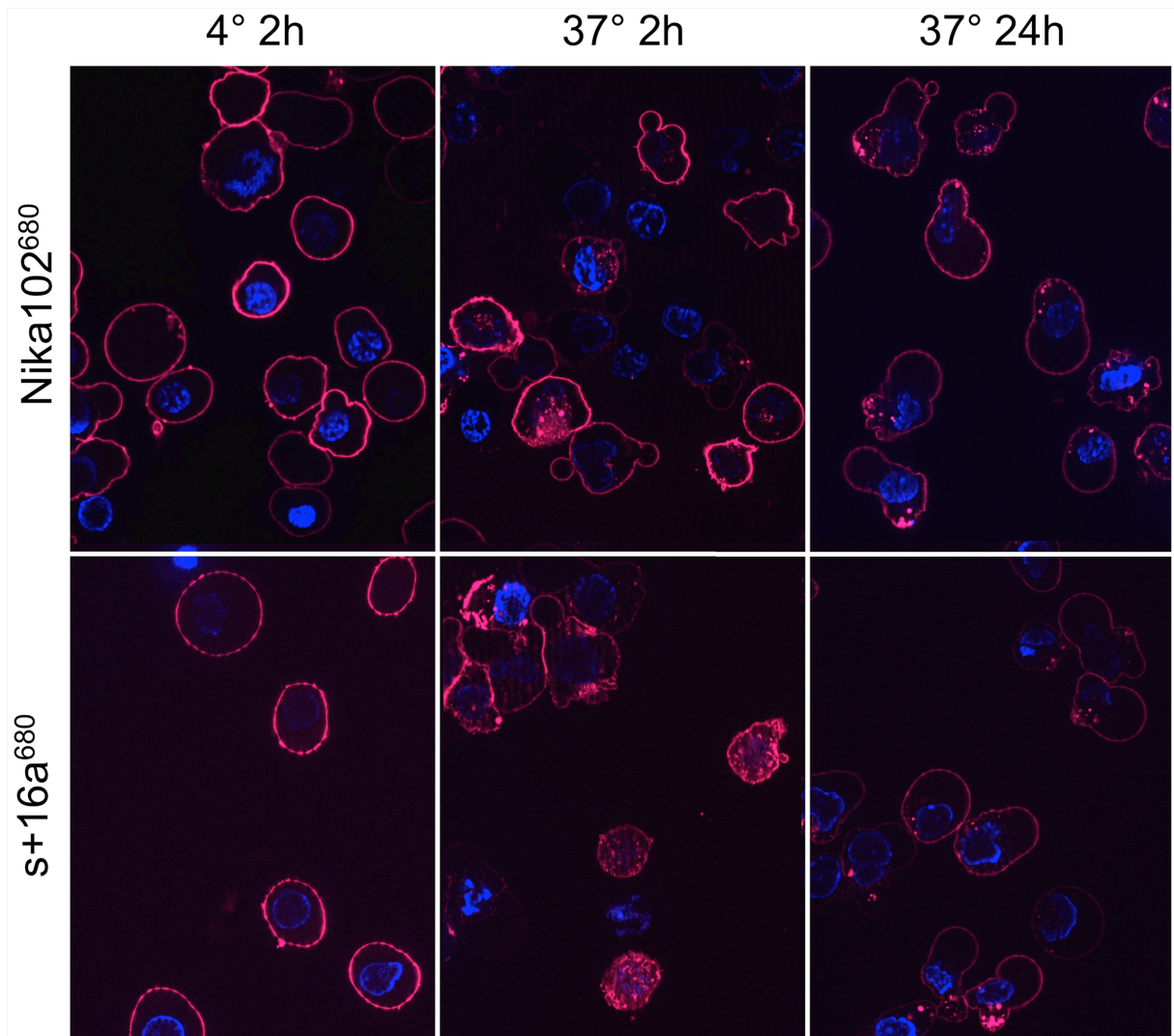
- Hoffman JM, Gambhir SS. Molecular imaging: the vision and opportunity for radiology in the future. *Radiology* 2007; 244(1): 39–47.
- Frangioni JV. New technologies for human cancer imaging. *J Clin Oncol* 2008; 26(24): 4012–4021.
- Wu AM, Olafsen T. Antibodies for molecular imaging of cancer. *Cancer J* 2008; 14(3): 191–197.
- Lisy MR, Goermer A, Thomas C, Pauli J, Resch-Genger U, Kaiser WA, Hilger I. *In vivo* near-infrared fluorescence imaging of carcinoembryonic antigen-expressing tumor cells in mice. *Radiology* 2008; 247(3): 779–787.
- Wu AM. Antibodies and antimatter: the resurgence of immuno-PET. *J Nucl Med* 2009; 50(1): 2–5.
- Kaur S, Venktaraman G, Jain M, Senapati S, Garg PK, Batra SK. Recent trends in antibody-based oncologic imaging. *Cancer Lett* 2012; 315(2): 97–111.
- Kelloff GJ, Krohn KA, Larson SM, Weissleder R, Mankoff DA, Hoffman JM, Link JM, Guyton KZ, Eckelman WC, Scher HI, O'Shaughnessy J, Cheson BD, Sigman CC, Tatum JL, Mills GQ, Sullivan DC, Woodcock

- J. The progress and promise of molecular imaging probes in oncologic drug development. *Clin Cancer Res* 2005; 11(22): 7967–7985.
8. Holliger P, Hudson PJ. Engineered antibody fragments and the rise of single domains. *Nat Biotechnol* 2005; 23(9): 1126–1136.
  9. Hamers-Casterman C, Atarhouch T, Muyldermans S, Robinson G, Hamers C, Songa EB, Bendahman N, Hamers R. Naturally occurring antibodies devoid of light chains. *Nature* 1993; 363(6428): 446–448.
  10. Wesolowski J, Alzogaray V, Reyelt J, Unger M, Juarez K, Urrutia M, Cauerhff A, Danquah W, Rissiek B, Scheuplein F, Schwarz N, Adriouch S, Boyer O, Seman M, Licea A, Serreze DV, Goldbaum FA, Haag F, Koch-Nolte F. Single domain antibodies: promising experimental and therapeutic tools in infection and immunity. *Med Microbiol Immunol* 2009; 198(3): 157–174.
  11. Bannas P, Well L, Lenz A, Rissiek B, Haag F, Schmid J, Hochgrafe K, Trepel M, Adam G, Ittrich H, Koch-Nolte F. *In vivo* near-infrared fluorescence targeting of T cells: comparison of nanobodies and conventional monoclonal antibodies. *Contrast Media Mol Imaging* 2014; 9(2): 135–142.
  12. Vaneycken I, Devoogdt N, Van Gassen N, Vincke C, Xavier C, Wernery U, Muyldermans S, Lahoutte T, Cavelliers V. Preclinical screening of anti-HER2 nanobodies for molecular imaging of breast cancer. *FASEB J* 2011; 25(7): 2433–2446.
  13. Xavier C, Vaneycken I, D'Huyvetter M, Heemskerck J, Keyaerts M, Vincke C, Devoogdt N, Muyldermans S, Lahoutte T, Cavelliers V. Synthesis, preclinical validation, dosimetry, and toxicity of 68Ga-NOTA-anti-HER2 Nanobodies for iPET imaging of HER2 receptor expression in cancer. *J Nucl Med* 2013; 54(5): 776–784.
  14. Tchouate Gainkam LO, Keyaerts M, Cavelliers V, Devoogdt N, Vanhove C, Van Grunsven L, Muyldermans S, Lahoutte T. Correlation between epidermal growth factor receptor-specific nanobody uptake and tumor burden: a tool for noninvasive monitoring of tumor response to therapy. *Mol Imaging Biol* 2011; 13(5): 940–948.
  15. Vosjan MJ, Perk LR, Roovers RC, Visser GW, Stigter-van Walsum M, van Bergen En Henegouwen PM, van Dongen GA. Facile labelling of an anti-epidermal growth factor receptor Nanobody with 68Ga via a novel bifunctional desferal chelate for immuno-PET. *Eur J Nucl Med Mol Imaging* 2011; 38(4): 753–763.
  16. Oliveira S, Heukers R, Sornkom J, Kok RJ, van Bergen En Henegouwen PM. Targeting tumors with nanobodies for cancer imaging and therapy. *J Control Release* 2013; 172(3): 607–617.
  17. Kijanka M, Warnders FJ, El Khattabi M, Lub-de Hooge M, van Dam GM, Ntziachristos V, de Vries L, Oliveira S, van Bergen En Henegouwen PM. Rapid optical imaging of human breast tumour xenografts using anti-HER2 VHHS site-directly conjugated to IRDye 800CW for image-guided surgery. *Eur J Nucl Med Mol Imaging* 2013; 40(11): 1718–1729.
  18. Zaman MB, Baral TN, Jakubek ZJ, Zhang J, Wu X, Lai E, Whitfield D, Yu K. Single-domain antibody bioconjugated near-IR quantum dots for targeted cellular imaging of pancreatic cancer. *J Nanosci Nanotechnol* 2011; 11(5): 3757–3763.
  19. Oliveira S, van Dongen GA, Stigter-van Walsum M, Roovers RC, Stam JC, Mali W, van Diest PJ, van Bergen en Henegouwen PM. Rapid visualization of human tumor xenografts through optical imaging with a near-infrared fluorescent anti-epidermal growth factor receptor nanobody. *Mol Imaging* 2012; 11(1): 33–46.
  20. D'Huyvetter M, Vincke C, Xavier C, Aerts A, Impens N, Baatout S, De Raeve H, Muyldermans S, Cavelliers V, Devoogdt N, Lahoutte T. Targeted radionuclide therapy with A 177Lu-labeled anti-HER2 nanobody. *Theranostics* 2014; 4(7): 708–720.
  21. Mould DR, Sweeney KR. The pharmacokinetics and pharmacodynamics of monoclonal antibodies—mechanistic modeling applied to drug development. *Curr Opin Drug Discov Develop* 2007; 10(1): 84–96.
  22. Lammers T, Kiessling F, Hennink WE, Storm G. Drug targeting to tumors: principles, pitfalls and (pre-) clinical progress. *J Control Release* 2012; 161(2): 175–187.
  23. Jain RK, Stylianopoulos T. Delivering nanomedicine to solid tumors. *Nature Rev Clin Oncol* 2010; 7(11): 653–664.
  24. Koch-Nolte F, Duffy T, Nissen M, Kahl S, Killeen N, Ablamunits V, Haag F, Leiter EH. A new monoclonal antibody detects a developmentally regulated mouse ecto-ADP-ribosyltransferase on T cells: subset distribution, inbred strain variation, and modulation upon T cell activation. *J Immunol* 1999; 163(11): 6014–6022.
  25. Koch-Nolte F, Reyelt J, Schossow B, Schwarz N, Scheuplein F, Rothenburg S, Haag F, Alzogaray V, Cauerhff A, Goldbaum FA. Single domain antibodies from llama effectively and specifically block T cell ecto-ADP-ribosyltransferase ART2.2 *in vivo*. *FASEB J* 2007; 21(13): 3490–3498.
  26. Bannas P, Adriouch S, Kahl S, Braasch F, Haag F, Koch-Nolte F. Activity and specificity of toxin-related mouse T cell ecto-ADP-ribosyltransferase ART2.2 depends on its association with lipid rafts. *Blood* 2005; 105(9): 3663–3670.
  27. Bannas P, Graumann O, Balcerak P, Peldschus K, Kaul MG, Hohenberg H, Haag F, Adam G, Ittrich H, Koch-Nolte F. Quantitative magnetic resonance imaging of enzyme activity on the cell surface: *in vitro* and *in vivo* monitoring of ADP-ribosyltransferase 2 on T cells. *Mol Imaging* 2010; 9(4): 211–222.
  28. Bannas P, Scheuplein F, Well L, Hermans-Borgmeyer I, Haag F, Koch-Nolte F. Transgenic overexpression of toxin-related ecto-ADP-ribosyltransferase ART2.2 sensitizes T cells but not B cells to NAD-induced cell death. *Mol Immunol* 2011; 48(15–16): 1762–1770.
  29. Hottiger MO, Hassa PO, Luscher B, Schuler H, Koch-Nolte F. Toward a unified nomenclature for mammalian ADP-ribosyltransferases. *Trends Biochem Sci* 2010; 35(4): 208–219.
  30. Gainkam LO, Cavelliers V, Devoogdt N, Vanhove C, Xavier C, Boerman O, Muyldermans S, Bossuyt A, Lahoutte T. Localization, mechanism and reduction of renal retention of technetium-99 m labeled epidermal growth factor receptor-specific nanobody in mice. *Contrast Media Mol Imaging* 2011; 6(2): 85–92.

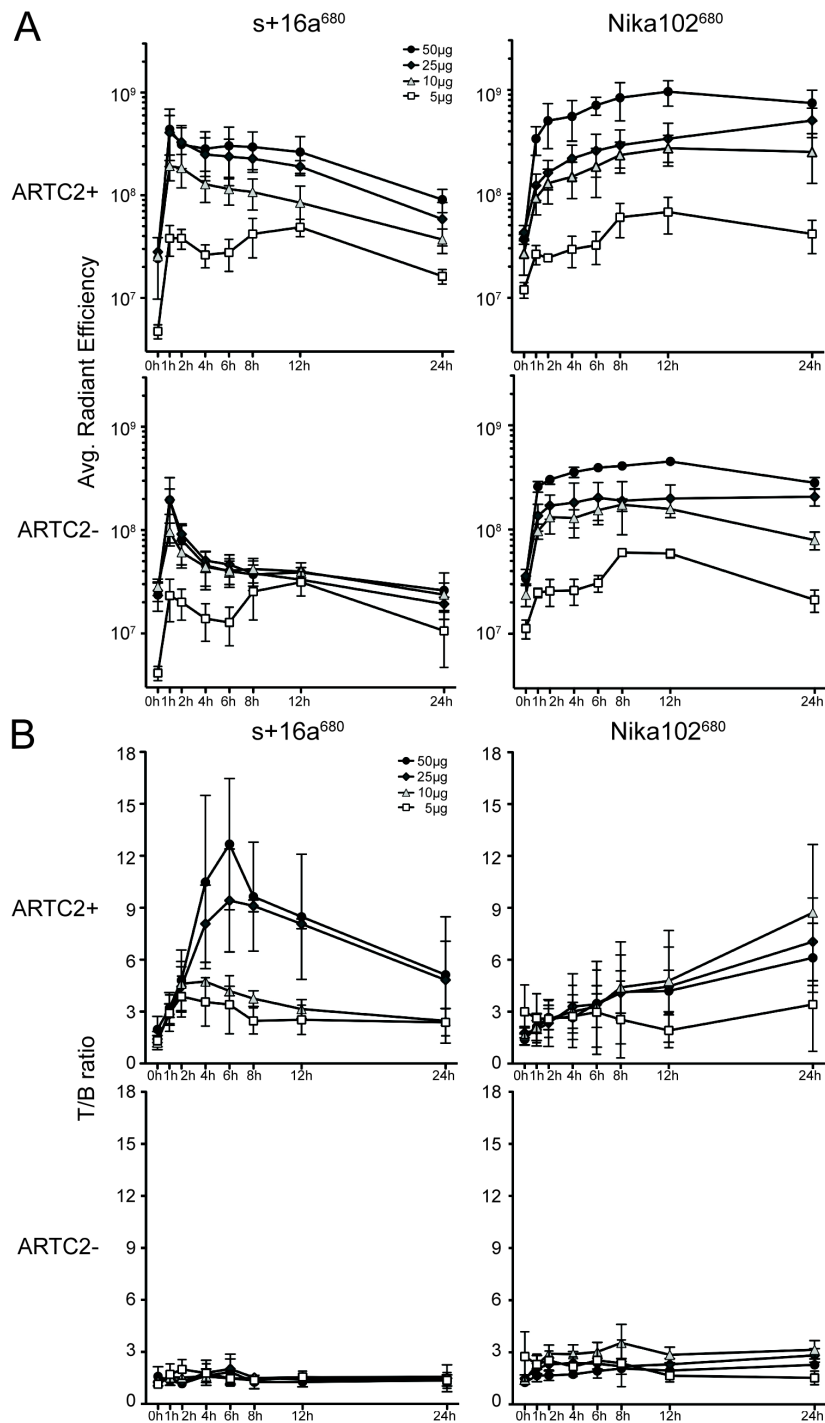
## SUPPORTING INFORMATION

Additional supporting information may be found in the online version of this article at the publisher's web site.

## 1.1 Supplementary tables and figures



**Supplementary Figure 1.** Internalization of s+16a<sup>680</sup> and Nika102<sup>680</sup>. DC27.10 ARTC2.2 cells were stained with s+16a<sup>680</sup> Nika102<sup>680</sup> for 30 min on ice and washed. Cells were further incubated in cell culture medium for the indicated times at 4°C or 37°C before fixation in 2% PFA, counterstaining with Hoechst 33428 and analysis by fluorescence microscopy.



**Supplementary Figure 2.** Comparative dose evaluation of s+16a<sup>680</sup> and Nika102<sup>680</sup> for *in vivo* NIRF-imaging. S+16a<sup>680</sup> and Nika102<sup>680</sup> were injected at a dose of 5 µg, 10 µg, 25 µg, or 50 µg into mice bearing both, ARTC2-positive and ARTC2-negative tumors. NIRF-imaging was performed at different time points after injection and ROIs were drawn around tumors and normal tissue (hind leg) for semi-quantitative analyses. (A) Radiant efficiencies and (B) calculated T/B-ratios of ARTC2-positive (upper panels) and ARTC2-negative (lower panels) tumors are plotted as a function of time.

## 2. Summary and description of the paper

Diagnostic imaging plays an essential role in the diagnosis and management of cancer. In recent years, technical advances of various imaging techniques have led to a widespread adoption in research and patient care. As a result there are now multiple imaging techniques, which supply information for screening, staging, therapy planning and monitoring (Fass 2008, Weissleder & Pittet 2008). Despite these technical advances and adoption of new equipment, there has not yet been a meaningful clinical impact. However, with emerging new imaging technologies, contrast agents, and biomarkers there is a great potential to improve patient care (Frangioni 2008, Fass 2008).

To better distinguish cancer cells from normal cells, and thus increase the sensitivity of detection, it is necessary to label the cells of interest with a specific contrast agent (Weissleder & Pittet 2008). The goal is to improve the signal-to-background ratio, which in return will have a positive impact on cancer screening, staging, and treatment (Frangioni 2008). The ideal imaging agent should accumulate in high concentrations at the sites of interest, while generating minimal non-specific background signal (Weissleder & Pittet 2008).

“Molecular imaging” is a relatively new discipline, which has gained tremendous momentum with recent advances in both molecular biology and imaging technology. Molecular imaging enables noninvasive imaging of molecular structures with specific contrast agents, thus enabling specific tumor targeting and visualization *in vivo*. This distinguishes molecular imaging from previous methods, which focused on providing gross anatomic or functional information. As an interdisciplinary research and clinical discipline it has the potential to drive advancements in diagnosis and monitoring of diseases, improving treatment and optimizing pre-clinical and clinical research (Kirchner & Willmann 2012, Hoffmann et al. 2007, Frangioni 2008). Commonly used technologies for molecular imaging include nuclear medicine diagnostics such as positron emission tomography (PET) and single photon computed tomography (SPECT). Near-infrared fluorescence (NIRF) imaging is another imaging technique, which has shown to be especially suited for preclinical molecular imaging. (Kirchner & Willmann 2012, Ntziachristos et al. 2003).

With NIRF-imaging, target antigens are labeled *in vivo* with fluorescent conjugated ligands (Ntziachristos et al. 2003). Fluorophores, which emit light in the near-infrared spectrum, can penetrate tissue up to several centimeters (Sosnovik et al. 2007). By labeling of fluorophores

to antibodies, it is possible to specifically detect cells *in vivo* (Lisy et al. 2008). Further, these probes are biocompatible, i.e. neither toxic nor immunogenic, which is important for clinical applications. These characteristics, in addition to a new wave of antibody based imaging approaches have already led to the clinical adoption of the NIRF-technology (van Dam et al. 2011, Terwisscha van Scheltinga et al. 2001).

Recombinant antibodies are a thriving and dynamic research field. Especially in cancer research, diagnostics, and therapy there has recently been a lot of progress (Holliger and Hudson 2005, Revets et al. 2005, Majidi et al. 2009). Antibodies are perfectly suited probes because they enable specific detection of cell-bound target proteins on cancer cells *in vivo* (Frenzel et al. 2013). To be successfully deployed in diagnostics and therapy, tumor-specific antibodies have to reach their target cells efficiently. For optimal tumor-targeting it is necessary for antibodies to have a high affinity to tumor cells but not to healthy cells. Furthermore, the total amount of unbound and free circulating antibodies should be as low as possible to minimize confounding non-specific signals (Holliger and Hudson 2005, Revets et al. 2005, Majidi et al. 2009). Tumor-targeting is predominantly affected by the structural characteristics of the antibody molecules themselves (Ghetie et al. 1997, Baudino et al. 2008, Stavenhagen et al. 2007). Furthermore, their molecular size of 150 kDa influences tissue permeability and retention in the kidneys (Tijink et al. 2008, Bell et al. 2010). The tumor tissue itself has an increased interstitial pressure, which in turn counteracts the permeation of larger molecules (Heine et al. 2012). These characteristics of conventional antibodies impair the signal-to background ratio, which is highly important for diagnostic imaging (Kelloff et al. 2005). These shortcomings of conventional antibodies have led to the development of new, genetically engineered forms of antibodies, such as diabodies, minibodies, single-chain variable fragments, and nanobodies (Wu and Olafsen 2008, Wu 2009, Kaur et al. 2012, Holliger and Hudson 2005).

Single-domain antibodies, or nanobodies, are a class of recombinantly expressed antibody fragments, which are engineered from heavy-chain-antibodies found in camelids and sharks. They offer the same specificity as conventional antibodies but can be produced more economically. Nanobodies have a low molecular mass (15 kDa), good bioavailability, low immunogenicity, fast renal elimination, and show good tissue penetration *in vivo*. (Hamers-Casterman et al. 1993, Wesolowski et al. 2009, Jain et al. 2007). This makes them perfectly suited for the specific detection of tumor antigens *in vivo* (Vaneycken et al. 2011, Xavier et al.

2013, Gainkam et al. 2011, Vosjan et al. 2011, Oliveira et al. 2013, Kijanka et al. 2013, Zaman et al. 2011, Oliveira et al. 2012, D'Huyvetter et al. 2014).

Several studies have shown that nanobodies allow higher tumor-to-background (T/B) ratios in molecular imaging applications than conventional antibodies (Kijanka et al. 2013, Oliveira et al. 2012). Although these results are promising, there are only few studies directly comparing nanobodies and conventional antibodies for molecular imaging applications *in vivo*.

When imaging tumor cells, the T/B-ratio depends mostly on the specificity of the antibody-constructs as well as the clearance of unbound antibody-constructs from the body. Both parameters depend largely on the molecular size of the probe. Therefore, different kinetics of accumulation and elimination from circulation for differently sized antibody-constructs have to be taken into account (Bannas et al. 2014). We aimed to further characterize the advantages and disadvantages of both nanobodies and conventional antibodies for their application in NIRF-imaging of tumors *in vivo*. We focused specifically on parameters that preceding studies failed to adjust for. This includes determining and comparing the optimum timing and dosage for imaging of tumors.

We compared a single-domain nanobody (s+16a, 17 kDa) and a monoclonal antibody (Nika102, 150 kDa), which were conjugated to the fluorescent dye AlexaFluor-680 (AF680). Both antibody-constructs are directed to ADP-ribosyltransferase ARTC2, which we chose as model target antigen. ARTC2 is expressed on the surface of lymphoma cells (Koch-Nolte et al. 2007, Bannas et al. 2005, Bannas et al. 2010, Bannas et al. 2011, Hottiger et al. 2010). For our subcutaneous tumor xenograft experiments we used athymic nude mice (NMRI-Foxn1<sup>nu</sup>). Mice were injected with ARTC2-transfected and ARTC2-untransfected DC27.10 murine lymphoma cells on the opposite flanks of the same animals. Imaging experiments were performed 7-9 days after injection, when tumors had reached a diameter of ~8 mm.

We hypothesized that it is essential to adjust the injected doses and imaging time points when comparing differently sized antibody-constructs for optimized tumor imaging. To determine the best imaging condition for each individual antibody-construct, we injected s+16a<sup>680</sup> and Nika102<sup>680</sup> intravenously into mice at different doses (5, 10, 25, and 50 µg). NIRF-imaging was performed before and after injection over a 24h period (Fig. 3 paper).

Our results revealed that labeling of ARTC2-positive tumors was specific with both nanobodies and antibodies. The signal was already strong at early time points with nanobody s+16a<sup>680</sup> and declined over time, whereas the antibody Nika102<sup>680</sup> showed a slowly increasing signal over 24-hours. The comparison of different doses of AF680-conjugates showed best imaging results with 50 µg of s+16a<sup>680</sup> and with 10 µg of Nika102<sup>680</sup>. With these doses we achieved highest specific signal intensities with s+16a<sup>680</sup>, while maintaining sufficient specific signals with Nika102<sup>680</sup>. In addition, we could minimize unspecific signals in ARTC2-negative tumors and background signals from unbound circulating AF680-conjugates. We observed a maximum T/B-ratio of 12 in ARTC2-positive tumors with 50 µg of s+16a<sup>680</sup> already 4-6 hours after injection, while 10µg of Nika102<sup>680</sup> showed a maximum T/B-ratio of 9 only 24 hours after injection (see Fig. 4 paper).

To evaluate the biodistribution und penetration of injected nanobodies and antibodies into the tumor tissue, we established a new validation technique (Fig. 1). We explanted the tumors and analyzed them *ex vivo* with both flow cytometry (see Fig. 8 paper) and fluorescence microscopy (see Fig. 9 paper). With both antibody-constructs being conjugated to the fluorescent dye AF680 we were able to detect signals without the need to use secondary reagents. For flow cytometry one tumor half was meshed through a cell strainer to obtain single cell suspensions. Flow cytometry allowed quantifying the fraction of labeled tumor cells, as well as the binding efficiency on tumor cells. The other half of the tumor was fixed and frozen on dry ice. For analysis with fluorescent microscopy we prepared sections of 8 µm, which were stained with DAPI to visualize nuclei and anti-CD31<sup>AF488</sup> to visualize vessels.

*Ex vivo* flow cytometry confirmed specific labeling of ARTC2-positive tumor cells, but not ARTC2-negative cells. Both flow cytometry and fluorescent microscopy showed a marked percentage of labeled cells at earlier time points with nanobody s+16a<sup>680</sup> compared to conventional antibody Nika102<sup>680</sup>. Fluorescent microscopy revealed a clear membranous staining of tumor cells. While nanobody s+16a<sup>680</sup> showed a significantly deeper penetration of tumor tissue, conventional antibody Nika102<sup>680</sup> showed clusters of labeled cells near the tumor vessels. We observed a clear decline in signal strength and labeling efficiency of tumors with s+16a<sup>680</sup> already 6 hours after injection. Nika102<sup>680</sup> on the other hand showed a steady increase in signal strength and labeling efficiency over 24 hours.

Our results confirm the hypothesis concerning the different behavior of differently sized antibody constructs *in vivo*. The smaller nanobodies proved to be ideal for molecular imaging purposes because they can be administered in high doses, penetrate the target tissue thoroughly, and excess is cleared rapidly from circulation via the kidneys. This leads to maximized specific signals of the tumors, with minimal unspecific signal from unbound circulating conjugates. In contrast, the conventional antibody showed that a high dosage leads to an excess of free circulating antibody, while offering less thorough penetration of the tumor. This leads to higher unspecific signals and lower T/B-ratios compared to nanobodies. However, the T/B-ratio of conventional antibodies could be improved at later time points by using lower doses of antibody conjugates.

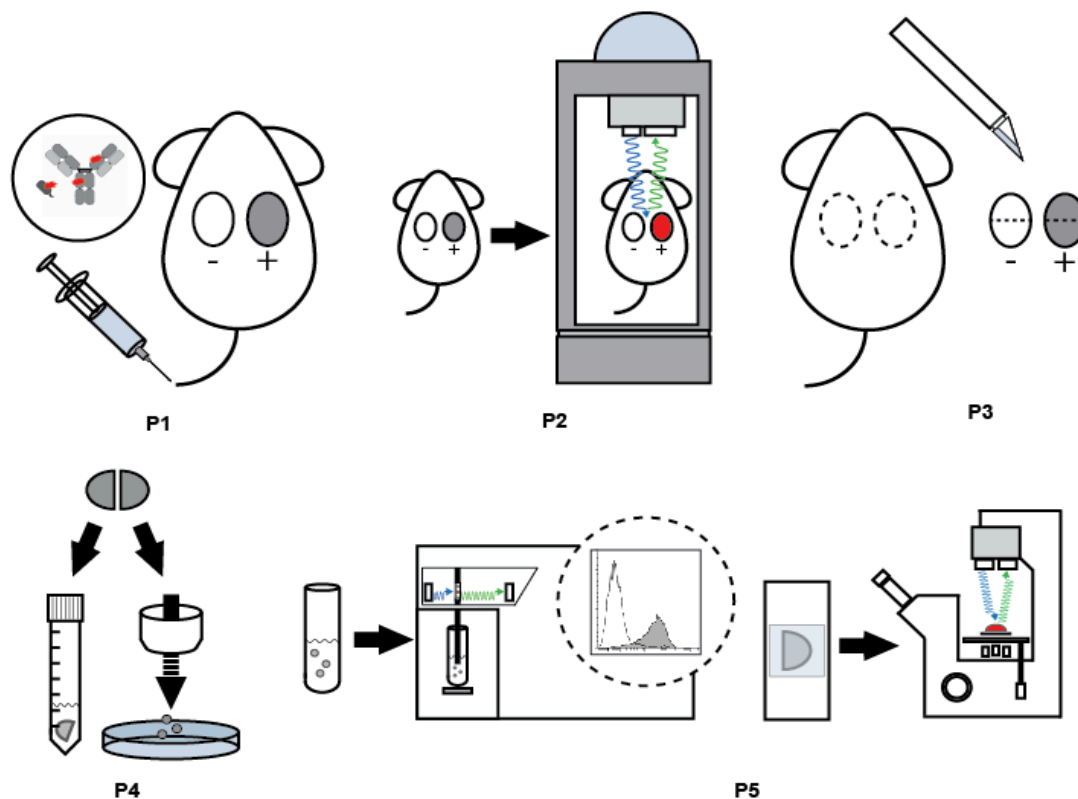


**Fig.1 Ex vivo validation of *in vivo* near-infrared fluorescence xenograft imaging experiments in mice.** At first, near-infrared fluorophore labeled antigen-specific nanobodies and conventional antibodies are administered to mice bearing both antigen-positive and -negative xenografts (P1). The second step is to perform *in vivo* imaging (P2). After imaging the mice are sacrificed to remove the xenografts (P3), which are processed for *ex vivo* analyses (P4). Ultimately, *ex vivo* flow cytometry and fluorescence microscopy are used to validate *in vivo* imaging results (P5). (Adapted from Bannas, Lenz et al. 2015)

In conclusion, we demonstrated that nanobodies are well suited as diagnostic tools for rapid and specific *in vivo* detection of lymphomas. Especially for same-day imaging purposes nanobodies are superior to conventional antibodies because they offer superior tissue penetration and significantly higher T/B-ratios. Our results are in accord with two recent studies, which used fluorophore-labeled nanobodies (Oliveira et al. 2012) and compared nanobodies and antibodies for PET imaging of xenograft models (Vosjan et al. 2011). Our experiments expand previous observations by showing that optimization of timing and dosing for each individual antibody construct has dramatic effects on the result of imaging experiments. Moreover, the use of a NIRF-dye allowed not only for *in vivo* imaging but also allowed to perform *ex vivo* validation experiments via flow cytometry and fluorescence microscopy.

The established methods in this project have model character and can be translated for clinical antibody- and nanobody-based specific molecular imaging of tumors. We believe that in the near future non-invasive *in vivo* molecular imaging with optimized recombinant antibodies will help to detect diseases earlier.

## 2.1 References

- Bannas P**, Adriouch S, Kahl S, Braasch F, Haag F, Koch-Nolte F. Activity and specificity of toxin-related mouse T cell ecto-ADP-ribosyltransferase ART2.2 depends on its association with lipid rafts. *Blood*. 2005;105(9):3663–70.
- Bannas P**, Graumann O, Balcerak P, Peldschus K, Kaul MG, Hohenberg H, et al. Quantitative magnetic resonance imaging of enzyme activity on the cell surface : In vitro and in vivo monitoring of ADP-Ribosyltransferase 2 on T cells. *Mol Imaging*. 2010;9(4):211–22.
- Bannas P**, Lenz A, Kunick V, Fumey W, Rissiek B, Schmid J, et al. Validation of nanobody and antibody based in vivo tumor xenograft NIRF-imaging experiments in mice using ex vivo flow cytometry and microscopy. *J Vis Exp*. 2015;(98):1–9.
- Bannas P**, Scheuplein F, Well L, Hermans-Borgmeyer I, Haag F, Koch-Nolte F. Transgenic overexpression of toxin-related ecto-ADP-ribosyltransferase ART2.2 sensitizes T cells but not B cells to NAD-induced cell death. *Mol Immunol*. 2011;(15-16):1762-70.
- Bannas P**, Well L, Lenz A, Rissiek B, Haag F, Schmid J, et al. In vivo near-infrared fluorescence targeting of T cells: comparison of nanobodies and conventional monoclonal antibodies. *Contrast Media Mol Imaging*. 2013;(2):135-42.
- Baudino L**, Shinohara Y, Nimmerjahn F, Furukawa J-I, Nakata M, Martinez-Soria E, et al. Crucial Role of Aspartic Acid at Position 265 in the CH2 Domain for Murine IgG2a and IgG2b Fc-Associated Effector Functions. *J Immunol*. 2008;(9):6664–9.
- Bell A**, Wang ZJ, Arbabi-Ghahroudi M, Chang T a., Durocher Y, Trojahn U, et al. Differential tumor-targeting abilities of three single-domain antibody formats. *Cancer Lett*. 2010;289(1):81–90.
- D’Huyvetter M**, Vincke C, Xavier C, Aerts A, Impens N, Baatout S, et al. Targeted Radionuclide Therapy with A 177 Lu-labeled Anti-HER2 Nanobody. *Theranostics*. 2014;4(7):708–20.
- Fass L**. Imaging and cancer: A review. *Mol Oncol*. 2008;2(2):115–52.
- Frangioni J V**. New technologies for human cancer imaging. *Journal of Clinical Oncology*. 2008;26(24):4012-21.
- Frenzel A**, Hust M, Schirrmann T. Expression of Recombinant Antibodies. *Front Immunol*. 2013;4:217.
- Gainkam LOT**, Keyaerts M, Caveliers V, Devoogdt N, Vanhove C, Van Grunsven L, et al. Correlation between epidermal growth factor receptor-specific nanobody uptake and tumor burden: A tool for noninvasive monitoring of tumor response to therapy. *Mol Imaging Biol*. 2011;13(5):940–8.
- Gambhir SS**. Just what is Molecular Imaging. *MI Gatew*. 2007;1:5-7.

**Ghetie V**, Popov S, Borvak J, Radu C, Matesoi D, Medesan C, Ober RJ WE. Increasing the serum persistence of an IgG fragment by random mutagenesis. *Nat Biotechnol.* 1997;15(7):328–30.

**Hamers-Casterman C**, Atarhouch T. Naturally occurring antibodies devoid of light chains. *Nature.* 1993;363:446–8.

**Heine M**, Freund B, Nielsen P, Jung C, Reimer R, Hohenberg H, et al. High interstitial fluid pressure is associated with low tumour penetration of diagnostic monoclonal antibodies applied for molecular imaging purposes. *PLoS One.* 2012;7(5):e36258.

**Hoffman JM**, Gambhir SS. Molecular imaging: the vision and opportunity for radiology in the future. *Radiology.* 2007; 244(1):39-47.

**Holliger P**, Hudson PJ. Engineered antibody fragments and the rise of single domains. *Nat Biotechnol.* 2005;23(9):1126-36.

**Hottiger MO**, Hassa PO, Lu B, Schu H. Toward a unified nomenclature for mammalian ADP-ribosyltransferases. *Trends Biochem Sci.* 2010; 35(4):208-19.

**Kaur S**, Venktaraman G, Jain M, Senapati S, Garg PK, Batra SK. Recent trends in antibody-based oncologic imaging. *Cancer Letters.* 2012; 315(2):97-111.

**Kelloff GJ**, Krohn KA, Larson SM, Weissleder R, Mankoff DA, Hoffman JM, et al. The progress and promise of molecular imaging probes in oncologic drug development. *Clinical Cancer Research.* 2005;11(22):7967-85.

**Kijanka M**, Dorresteijn B, Oliveira S, Henegouwen PMVBE. Nanobody-based cancer therapy of solid tumors. *Nanomedicine.* 2015;10:161–74.

**Kijanka M**, Warnders F-J, El Khattabi M, Lub-de Hooge M, van Dam GM, Ntziachristos V, et al. Rapid optical imaging of human breast tumour xenografts using anti-HER2 VHHs site-directly conjugated to IRDye 800CW for image-guided surgery. *Eur J Nucl Med Mol Imaging.* 2013;40(11):1718–29.

**Kircher MF**, Willmann JK. Molecular Body Imaging : MR Imaging, CT, and US. Part I. Principles. *Radiology.* 2012;264(2):349–68.

**Koch-Nolte F**, Reyelt J, Schössow B, Schwarz N, Scheuplein F, Rothenburg S, et al. Single domain antibodies from llama effectively and specifically block T cell ecto-ADP-ribosyltransferase ART2.2 in vivo. *FASEB J.* 2007;21(13):3490–8.

**Lisy M-R**, Goermar A, Thomas C, Pauli J, Resch-Genger U, Kaiser WA, et al. In vivo near-infrared fluorescence imaging of carcinoembryonic antigen-expressing tumor cells in mice. *Radiology.* 2008;247(3):779–87.

**Majidi J**, Barar J, Baradaran B, Abdolalizadeh J, Omid Y. Target therapy of cancer: Implementation of monoclonal antibodies and nanobodies. *Hum Antibodies.* 2009;18(3):81–100.

**Ntziachristos V**, Bremer C, Weissleder R. Fluorescence imaging with near-infrared light: new technological advances that enable in vivo molecular imaging. *Eur Radiol.* 2003;13(1):195–208.

**Oliveira S**, Heukers R, Sornkom J, Kok RJ, van Bergen En Henegouwen PMP. Targeting tumors with nanobodies for cancer imaging and therapy. *J Control Release.* 2013; 172(3):607–17.

**Oliveira S**, van Dongen G a MS, Stigter-van Walsum M, Roovers RC, Stam JC, Mali W, et al. Rapid Visualization of Human Tumor Xenografts through Optical Imaging with a Near-infrared Fluorescent Anti-Epidermal Growth Factor Receptor Nanobody. *Mol Imaging.* 2012;11(1):33–46.

**Revets H**, Baetselier P De, Muyldermans S, Publications A. Nanobodies as novel agents for cancer therapy. *Expert Opin Biol Ther.* 2005;5(1):111–24.

**Sosnovik DE**, Nahrendorf M, Deliolanis N, Novikov M, Aikawa E, Josephson L, et al. Fluorescence Tomography and Magnetic Resonance Imaging of Myocardial Macrophage Infiltration in Infarcted Myocardium In Vivo. *Circulation.* 2007;115(11):1384–91.

**Stavenhagen JB**, Gorlatov S, Tuailon N, Rankin CT, Li H, Burke S, et al. Fc Optimization of Therapeutic Antibodies Enhances Their Ability to Kill Tumor Cells In vitro and Controls Tumor Expansion In vivo via Low-Affinity Activating Fc Receptors. *Cancer Res.* 2007;67(18):8882–90.

**Terwisscha van Scheltinga AGT**, van Dam GM, Nagengast WB, Ntziachristos V, Hollema H, Herek JL, et al. Intraoperative near-infrared fluorescence tumor imaging with vascular endothelial growth factor and human epidermal growth factor receptor 2 targeting antibodies. *J Nucl Med.* 2011;52(11):1778–85.

**Tijink BM**, Laeremans T, Budde M, Stigter-van Walsum M, Dreier T, de Haard HJ, et al. Improved tumor targeting of anti-epidermal growth factor receptor Nanobodies through albumin binding: taking advantage of modular Nanobody technology. *Mol Cancer Ther.* 2008;7(8):2288–97.

**van Dam GM**, Themelis G, Crane LM a, Harlaar NJ, Pleijhuis RG, Kelder W, et al. Intraoperative tumor-specific fluorescence imaging in ovarian cancer by folate receptor- $\alpha$  targeting: first in-human results. *Nat Med.* 2011;17(10):1315–9.

**Vaneycken I**, Devoogdt N, Gassen N Van, Xavier C, Wernery U, Muyldermans S, et al. Preclinical screening of anti-HER2 nanobodies for molecular imaging of breast cancer. *FASEB J.* 2011;25(7):2433–46.

**Vosjan MJWD**, Perk LR, Roovers RC, Visser GWM, Walsum MS, Bergen PMP Van. Facile labelling of an anti-epidermal growth factor receptor Nanobody with  $^{68}\text{Ga}$  via a novel bifunctional desferal chelate for immuno-PET. *Eur J Nucl Med Mol Imaging.* 2011;753–63.

**Weissleder R**, Pittet MJ. Imaging in the era of molecular oncology. *Nature.* 2008;452(7187):580–9.

**Wesolowski J**, Alzogaray V, Reyelt J, Unger M, Juarez K, Urrutia M, et al. Single domain antibodies: promising experimental and therapeutic tools in infection and immunity. *Med Microbiol Immunol.* 2009;198(3):157–74.

**Wu AM.** Antibodies and antimatter: the resurgence of immuno-PET. *J Nucl Med.* 2009;50(1):2–5.

**Wu AM**, Olafsen T. Antibodies for molecular imaging of cancer. *Cancer J.* 2008;14(3):191-7.

**Xavier C**, Vaneycken I, Matthias D, Heemskerk J, Keyaerts M, Vincke C, et al. Synthesis, Preclinical Validation, Dosimetry, and Toxicity of <sup>68</sup>Ga-NOTA-Anti-HER2 Nanobodies for iPET Imaging of HER2 Receptor Expression in Cancer. *J Nucl Med.* 2013;54(5):776–85.

**Zaman MB**, Baral TN, Jakubek ZJ, Zhang J, Wu X, Lai E, Whitfield D, Yu K. Single-Domain Antibody Bioconjugated Near-IR Quantum Dots for Targeted Cellular Imaging of Pancreatic Cancer. *J Nanosci Nanotechnol.* 2011;11(5):3757–63(7).

### 3. Abstract

The utility of nanobodies and conventional antibodies for *in vivo* imaging is well known, but optimum dosing and timing schedules for one versus the other have not been established. We aimed to improve specific tumor imaging *in vivo* with nanobodies and conventional antibodies using near-infrared fluorescence (NIRF) imaging. We used ARTC2 expressed on lymphoma cells as a model target antigen. ARTC2-specific nanobody s+16a and conventional antibody Nika102 were labeled with NIRF-dye AF680. *In vivo* NIRF-imaging of ARTC2-positive and ARTC2-negative xenografts was performed over 24 h post-injection of 5, 10, 25, or 50 µg of each conjugate. Specific target-binding and tissue-penetration were verified by NIRF imaging *ex vivo*, flow cytometry and fluorescence microscopy. NIRF imaging of s+16a<sup>680</sup> *in vivo* revealed a six times faster tumor accumulation than of Nika102<sup>680</sup>. Using 50 µg of s+16a<sup>680</sup> increased the specific signals of ARTC2-positive tumors without increasing background signals, allowing a tumor-to-background (T/B) ratio of  $12.4 \pm 4.2$  within 6 h post-injection. Fifty micrograms of Nika102<sup>680</sup> increased specific signals of ARTC2-positive tumors but also of ARTC2-negative tumors and background, thereby limiting the T/B-ratio to  $6.1 \pm 2.0$ . Ten micrograms of Nika102<sup>680</sup> only slightly reduced specific tumor signals but dramatically reduced background signals. *Ex vivo* analyses confirmed a faster and deeper tumor penetration with s+16a<sup>680</sup>. Using nanobody s+16a allowed same-day imaging with a high T/B-ratio, whereas antibody Nika102 gave optimal imaging results only 24 h post injection. Nanobody s+16a required a high dose, whereas antibody Nika102 had the best T/B-ratio at a low dose. Therefore, timing and dosage should be addressed when comparing nanobodies and conventional antibodies for molecular imaging purposes.

Der Nutzen von Nanobodies und konventionellen Antikörpern für die *in vivo* Bildgebung ist bekannt. Jedoch sind in der Anwendung weder optimale Dosierungen noch Zeitabläufe etabliert. Wir haben uns zum Ziel gesetzt, die spezifische *in vivo* Nah-Infrarot-Fluoreszenzbildgebung (NIRF) von Tumoren mittels Nanobodies und konventionellen Antikörpern zu optimieren. Als Modell-Antigen haben wir das auf Lymphomzellen exprimierte ARTC2 verwendet. Der ARTC2-spezifische Nanobody s+16a und der konventionelle Antikörper Nika102 wurden mit dem NIRF-Farbstoff AF680 konjugiert. Nach Injektion von jeweils 5, 10, 25 oder 50 µg jedes Konjugats wurden *in vivo* NIRF-Bildgebungsversuche mit ARTC2-positiven und negativen Xenografts über einen Zeitraum von 24 h durchgeführt. Die spezifische Bindung an Zielstrukturen und Gewebsdurchgängigkeit wurden mittels *ex vivo* NIRF-Bildgebung, Durchflusszytometrie und Fluoreszenzmikroskopie verifiziert. NIRF-Bildgebung *in vivo* von s+16a<sup>680</sup> zeigte eine sechsfach schnellere Tumoranreicherung im Vergleich zu Nika102<sup>680</sup>. Durch die Verwendung von 50 µg s+16a<sup>680</sup> ließen sich die spezifischen Signale der ARTC2-positiven Tumoren steigern, ohne unspezifische Hintergrundsignale zu erhöhen. So konnte ein Tumor-zu-Hintergrund (T/B) Verhältnis von  $12.4 \pm 4.2$  innerhalb von 6 h erreicht werden. Fünfzig µg von Nika102<sup>680</sup> erhöhten das spezifische Tumorsignal von ARTC2-positiven Tumoren, bei jedoch gleichzeitiger Erhöhung des Signals der ARTC2-negativen Tumoren und des Hintergrundsignals. Dadurch ergab sich ein reduziertes T/B-Verhältnis von nur  $6.1 \pm 2.0$ . Der Einsatz von 10 µg Nika102<sup>680</sup> hatten nur eine geringe Reduktion des spezifischen Signals zu folge, konnten jedoch das Hintergrundsignal drastisch reduzieren. Die *ex vivo* Analyse konnten eine schnellere und tiefere Tumorpenetration mit s+16a<sup>680</sup> bestätigen. Der Nanobody s+16a ermöglichte Bildgebung am Injektionstag mit einem hohen T/B-Verhältnis, wohingegen der Antikörper Nika102 die besten Ergebnisse erst 24 h nach Injektion zeigte. Der Nanobody s+16a benötigte hohe Dosen, wohingegen der Antikörper Nika102 die T/B-Verhältnisse mit niedrigen Dosen erzielen konnte. Eine Anpassung der Dosis und Zeitabläufe ist daher essentiell für vergleichende Versuche mit Nanobodies und konventionellen Antikörpern in der molekularen Bildgebung.

#### 4. Explanation of own contribution

Molecular imaging of tumors with nanobodies and antibodies: Timing and dosage are crucial factors for improved *in vivo* detection

**Bannas P\***, **Lenz A\***, Kunick V, Well L, Fumey W, Rissiek B, Haag F, Schmid J, Schütze K, Eichhoff A, Trepel M, Adam G, Ittrich H and Koch-Nolte F.

*Contrast Media Mol. Imaging*. Accepted February 3rd, 2015

\*The first two authors contributed equally.

Impact Factor: 2.923 (2014)

The schematic illustration shown in Fig. 1a was created by Dr. med. Bannas. Mrs. Schmid made the coomassie-stained gel in Fig. 1b and performed the experiments for Fig. 1c and 1d. The doctoral candidate performed the corresponding imaging experiments for Fig. 1b, 1c and 1d. All imaging experiments with the IVIS imaging system were performed with the help of the staff from the Core Facility in-vivo-Optical-Imaging at the Universitätsklinikum Hamburg-Eppendorf (UKE). Experiments shown in Fig. 2 were performed by the doctoral candidate. Animal handling and preparation of organs for experiments shown in Fig. 3 were performed by and under supervision of the doctoral candidate with the help of Mrs. Schmid, Mr. Kunick, and Mr. Fumey. Intravenous injections were performed by the doctoral candidate. Statistical analyses for Fig. 5 to Fig. 8 and supplementary Fig. 2 were performed by the doctoral candidate. Fluorescence microscopy experiments in Fig. 9 were performed by the doctoral candidate with help from the staff of the UKE Microscopy Imaging Facility (UMIF). Imaging experiments in supplementary Fig. 1 were performed by Ms. Schütze and Ms. Eichhoff. Mr. Well and Dr. rer. nat. Rissiek contributed with their expertise concerning antibodies and animal handling. Conjugation of antibodies was performed by Mrs. Schmid. Prof. Dr. med. Trepel provided the technical equipment for the NIRF-imaging experiments. The doctoral candidate was responsible for planning, execution and analysis of the experiments. Except Fig. 1, all illustrations were created by the doctoral candidate. The doctoral candidate was involved in drafting the study design, which was conceived by Dr. med. Peter Bannas and Prof. Dr. med. Koch-Nolte, and drafting the manuscript. Prof. Dr. med. Adam, Prof. Dr. med. Haag, Prof. Dr. med. Trepel and PD. Dr. med. Ittrich provided their expertise during the study and the revision of the manuscript. All authors were involved in the revision of the manuscript.

## 5. Acknowledgements

First and foremost, I would like to express my gratitude to my supervisor Prof. Adam for giving me the opportunity to do my thesis in his department and for providing me with continuous support over the years.

I want to thank my advisor Prof. Nolte, who taught me everything there is to know about being a good researcher. His contribution of time, ideas and helpful instructions were essential for adjusting to the laboratory environment and understanding how research works.

A very special thanks goes out to my advisor and mentor PD. Dr. Bannas, whose expertise, understanding, and ideas, added considerably to my graduate experience. I am also grateful to him for providing a role model for me for being a dedicated clinician and researcher and for his attentive support.

I would like to thank Prof. Haag, Prof. Trepel and PD. Dr. Ittrich for their friendly support and critical advice.

The members of the AG Bannas and the research lab of the Department of Immunology have contributed immensely to my personal and professional time at the UKE. The group has been a source of friendship as well as good advice and collaboration. I am especially grateful for the help of Joanna Schmid, her outstanding technical support and her introduction to laboratory techniques. I thank Lennart Well and Valentin Kunick for their tremendous help during experiments. I also thank Björn Rissiek, Welbeck Danquah, and Stephan Menzel who were always willing to share their expertise and give helpful advice.

Also, I would like to thank all cooperation partners from other laboratory groups at the UKE for the close and successful collaboration, especially Dr. Leingärtner and Michael Horn-Glander of the In Vivo Imaging Core Facility for their help during the imaging experiments.

I gratefully recognize that this research would not have been possible without the financial assistance of the Department of Diagnostic and Interventional Radiology at the UKE, the Department of Immunology at the UKE, and the support of the graduate research school „Inflammation and Regeneration“ of the Deutsche Forschungsgemeinschaft (DFG).

Lastly, I would like to thank my parents Gabriele and Rainer Lenz, family and friends for the support they provided me throughout the entire process.

## **6. Curriculum Vitae**

Entfällt aus datenschutzrechtlichen Gründen.

## 7. Publications

### Publications

---

**Molecular imaging of tumors with nanobodies and antibodies: Timing and dosage are crucial factors for improved *in vivo* detection.**

Bannas P\*, Lenz A\*, Kunick V, Well L, Fumey W, Rissiek B, Haag F, Schmid J, Schütze K, Eichhoff A, Trepel M, Adam G, Ittrich H, Koch-Nolte F. Contrast Media Mol Imaging. 2015 Sep;10(5): 367-78. doi: 10.1002/cmimi.1637.

**Validation of nanobody and antibody based *in vivo* tumor xenograft NIRF-imaging experiments in mice using *ex vivo* flow cytometry and microscopy.**

Bannas P\*, Lenz A\*, Kunick V, Fumey W, Rissiek B, Schmid J, Haag F, Leingärtner A, Trepel M, Adam G, Koch-Nolte F, J Vis Exp. 2015 Apr 6;(98): e52462. doi: 10.3791/52462.

**In vivo near-infrared fluorescence targeting of T cells: Comparison of nanobodies and conventional monoclonal antibodies.**

Bannas P\*, Well L\*, Lenz A, Rissiek B, Haag F, Schmid J, Hochgräfe K, Trepel M, Adam G, Ittrich H, Koch-Nolte F. Contrast Media Mol Imaging. 2014 Mar-Apr;9(2): 135-42. doi: 10.1002/cmimi.1548.

### Conference Papers and Talks

---

**NIRF-Bildgebung von Lymphomen: Tumor-zu-Hintergrund-Ratio von Nanobodies und Antikörpern.**

Lenz A, Kunick V, Well L, Rissiek B, Haag F, Ittrich H, Adam G, Koch-Nolte F, Bannas P. Experimentelle Radiologie, Kiel, Germany 2012 (Talk)

**Comparison of nanobodies and conventional monoclonal antibodies for *in vivo* fluorescence imaging of lymphomas.**

Lenz A, Kunick V, Well L, Danquah W, Haag F, Trepel M, Adam G, Ittrich H, Koch-Nolte F, Bannas P. World Molecular Imaging Congress, Dublin, Ireland 2012 (Poster)

## **8. Eidesstattliche Versicherung**

Ich versichere ausdrücklich, dass ich die Arbeit selbständig und ohne fremde Hilfe verfasst, andere als die von mir angegebenen Quellen und Hilfsmittel nicht benutzt und die aus den benutzten Werken wörtlich oder inhaltlich entnommenen Stellen einzeln nach Ausgabe (Auflage und Jahr des Erscheinens), Band und Seite des benutzten Werkes kenntlich gemacht habe.

Ferner versichere ich, dass ich die Dissertation bisher nicht einem Fachvertreter an einer anderen Hochschule zur Überprüfung vorgelegt oder mich anderweitig um Zulassung zur Promotion beworben habe.

Ich erkläre mich einverstanden, dass meine Dissertation vom Dekanat der Medizinischen Fakultät mit einer gängigen Software zur Erkennung von Plagiaten überprüft werden kann.

Unterschrift: .....